Global Biogeochemical Cycles®

RESEARCH ARTICLE
10.1029/2021GB007160

Key Points:

- Peat particulate organic matter electron accepting and donating capacities per grams of carbon are smaller than for humic and fulvic acids
- Both capacities are small in highly decomposed peat, unless it has larger amounts of quinones and phenols
- We explain these patterns with parent vegetation chemistry and conditions during decomposition

Supporting Information:

Supporting Information may be found in the online version of this article.

Correspondence to:

K.-H. Knorr and C. Gao,
klaus-holger.knorr@uni-muenster.de;
gaochuanyu@iga.ac.cn

Citation:

Teickner, H., Gao, C., & Knorr, K.-H. (2022). Electrochemical properties of peat particulate organic matter on a global scale: Relation to peat chemistry and degree of decomposition. *Global Biogeochemical Cycles*, *36*, e2021GB007160. https://doi.org/10.1029/2021GB007160

Received 20 AUG 2021
Accepted 24 JAN 2022

Author Contributions:

Conceptualization: Henning Teickner, Chuanyu Gao, Klaus-Holger Knorr
Data curation: Henning Teickner
Formal analysis: Henning Teickner
Funding acquisition: Klaus-Holger Knorr
Investigation: Henning Teickner, Chuanyu Gao
Methodology: Chuanyu Gao, Klaus-Holger Knorr
Project Administration: Klaus-Holger Knorr
Resources: Klaus-Holger Knorr

Electrochemical Properties of Peat Particulate Organic Matter on a Global Scale: Relation to Peat Chemistry and Degree of Decomposition

Henning Teickner[1], Chuanyu Gao[1,2], and Klaus-Holger Knorr[1]

[1]ILÖK, Ecohydrology and Biogeochemistry Group, University of Münster, Münster, Germany, [2]Key Laboratory of Wetland Ecology and Environment, Northeast Institute of Geography and Agroecology, Chinese Academy of Sciences, Changchun, China

Abstract Methane production in peatlands is controlled by the availability of electron acceptors for microbial respiration, including peat dissolved organic matter (DOM) and particulate organic matter (POM). Despite the much larger mass of POM in peat, knowledge on the ranges of its electron transfer capacities—electron accepting capacity (EAC), and electron donating capacity (EDC)—is scarce in comparison to DOM and humic and fulvic acids. Moreover, it is unclear how peat POM chemistry and decomposition relate to its EAC and EDC. To address these knowledge gaps, we compiled peat samples with varying carbon contents from mid to high latitude peatlands and analyzed their EAC_{POM} and EDC_{POM}, element ratios, decomposition indicators, and relative amounts of molecular structures as derived from mid infrared spectra. Peat EAC_{POM} and EDC_{POM} are smaller (per gram carbon) than EAC and EDC of DOM and terrestrial and aquatic humic and fulvic acids and are highly variable within and between sites. Both are small in highly decomposed peat, unless it has larger amounts of quinones and phenols. Element ratio-based models failed to predict EAC_{POM} and EDC_{POM}, while mid infrared spectra-based models can predict peat EAC_{POM} to a large extent, but not EDC_{POM}. We suggest a conceptual model that describes how vegetation chemistry and decomposition control polymeric phenol and quinone contents as drivers of peat EDC_{POM} and EAC_{POM}. The conceptual model implies that we need mechanistic models or spatially resolved measurements to understand the variability in peat EDC_{POM} and EAC_{POM} and thus its role in controlling methane formation.

Plain Language Summary Peatlands accumulated large amounts of carbon via photosynthesis and slow decomposition of senesced plant material. Microorganisms within the peat form methane. For this reason, peatlands are important global sources of the greenhouse gas methane and therefore can contribute to climate change. In order to produce methane, the microorganisms have to transfer electrons between compounds in respiration processes. Only recently, it has been found that the peat itself can reversibly transfer electrons and that its capacities to reversibly accept electron accepting capacity (EAC) and reversibly donate electron donating capacity (EDC) electrons are large. We investigated which conditions favor large or small EAC and EDC of peat so that we can better explain methane formation. We argue that vegetation and decomposition control the amount of phenols and quinones—molecules in the peat that presumably are responsible for most of the peat's EAC and EDC. The EAC and EDC probably are largest for peat formed from vegetation rich in quinones and phenols, such as shrubs, and smaller for other vegetation types, for example, certain mosses. Intense decomposition may reduce both the EAC and EDC.

1. Introduction

Mid to high-latitude peatlands are important actors in the global carbon cycle with differential effects on the global climate (Frolking et al., 2011). On the one hand, they accumulated large amounts of atmospheric carbon dioxide (CO_2) in the form of peat (Limpens et al., 2008), on the other hand they produce large amounts of methane (CH_4) which can be emitted to the atmosphere (Frolking et al., 2011; Limpens et al., 2008). Redox reactions are important controls of carbon turnover and therefore redox processes and their role in methane and CO_2 production are crucial to understand peatland carbon dynamics (Limpens et al., 2008).

Methane formation is an obligatory anaerobic process and thus occurs only in the (at least temporally) anoxic zone of peatlands (Limpens et al., 2008). It can be suppressed if thermodynamically more favorable terminal electron acceptors (TEA), such as nitrate, iron oxides, sulphate, or organic molecules, are available (Blodau, 2011;

Software: Henning Teickner
Supervision: Klaus-Holger Knorr
Validation: Henning Teickner
Visualization: Henning Teickner
Writing – original draft: Henning Teickner, Klaus-Holger Knorr
Writing – review & editing: Henning Teickner, Chuanyu Gao, Klaus-Holger Knorr

Gao et al., 2019; Klüpfel et al., 2014). While inorganic TEAs typically have a comparatively small abundance in peatlands, suppression of CH_4 formation can occur due to the large abundance of OM that acts as TEA (Gao et al., 2019) and can be "recharged" even during short oxic periods (Klüpfel et al., 2014; Lau et al., 2016; Walpen, Lau, et al., 2018). Whereas dissolved organic matter (DOM) acts as electron mediator during such respiration processes (Gao et al., 2019; Lau et al., 2016), POM provides the main part of the electron accepting capacity (EAC) of peat and can continuously reoxidize DOM mediators and other TEAs (Blodau et al., 2007; Gao et al., 2019). Consequently, understanding the electrochemical properties of peat POM and how these are driven by vegetation chemistry and decomposition are key to understand CH_4 emissions from peatlands.

How OM chemistry controls its capacity to accept electrons electron donating capacity (EDC) has been studied mainly for DOM and humic and fulvic acids (Aeschbacher et al., 2012, 2010; Fimmen et al., 2007; Hernández-Montoya et al., 2012; LaCroix et al., 2020; Ratasuk & Nanny, 2007; Tan et al., 2017; Walpen, Getzinger, et al., 2018). The positive relation of the EAC to the C:H ratio and the EAC and EDC to indicators for aromaticity have been attributed to quinones and phenols representing the main contributors to the EAC and EDC, respectively (Aeschbacher et al., 2010; Tan et al., 2017). In addition, sulfur and nitrogen containing functional groups can contribute to the EAC and EDC (Fimmen et al., 2007; Hernández-Montoya et al., 2012; Ratasuk & Nanny, 2007) and the specific configuration of substituents and the degree of condensation control the magnitude and reversibility of the redox reactions (Ratasuk & Nanny, 2007; Uchimiya & Stone, 2009). Overall, there is a quite detailed conceptual understanding, which molecular structures are related to the EAC and EDC of DOM and humic and fulvic acids.

In contrast, knowledge on peat POM EAC and EDC (EAC_{POM} and EDC_{POM}) and even more on how peat POM chemistry relates to its EAC and EDC is still scarce. Few studies analyzed the EAC and EDC of POM (Gao et al., 2019; Keller & Takagi, 2013; Lau et al., 2015, 2016). These studies focused on quantifying and analyzing the reversibility of the electron transfer, but not how POM chemistry relates to its EAC and EDC (Gao et al., 2019; Keller & Takagi, 2013; Lau et al., 2015, 2016). However, the ranges of the EAC_{POM} and EDC_{POM} for peat POM are not sufficiently quantified yet. Furthermore, POM has different chemical properties than DOM and humic and fulvic acids because these fractions are derived from POM or represent subfractions of DOM which may be chemically altered (either via decomposition reactions—in case of DOM—and/or addition of acids and bases during extraction—in case of humic and fulvic acids; Lipczynska-Kochany, 2018; Worrall et al., 2017). Therefore, it is unclear if POM electrochemical properties correlate in the same way to element ratios or molecular structures as for DOM and humic and fulvic acids.

"Classical" indicators of peat chemistry (e.g., element ratios and the nominal oxidation state of carbon (C_{OX})), tools to infer the contribution of different OM fractions, such as lignin or polysaccharides, (e.g., van-Krevelen diagrams; Kim et al. (2003)) and measurement procedures (e.g., mid infrared spectroscopy) are promising techniques to explore how peat POM chemistry relates to its EAC and EDC. These methods have been widely used to analyze peat chemistry, its molecular structures, and electrochemical properties of DOM and humic and fulvic acids (Aeschbacher et al., 2010, 2012; Artz et al., 2008; Bader et al., 2018; Cocozza et al., 2003; Hodgkins et al., 2018; LaCroix et al., 2020; Leifeld et al., 2012, 2020; Lv et al., 2018; Moore et al., 2018; Tan et al., 2017; Tfaily et al., 2014; Worrall et al., 2017). Therefore, these approaches can be useful to analyze how different OM fractions and molecular structures in POM relate to its EAC and EDC.

Similarly unexplored are the relations between the degree of decomposition of peat and its EAC_{POM} and EDC_{POM}. Since decomposition can considerably transform peat POM and its molecular structures (Cocozza et al., 2003), it could have large effects on its EAC_{POM} and EDC_{POM}. Specifically, these may be irreversible changes of the EAC_{POM} and EDC_{POM} via decomposition and oxidation of polymeric phenol and quinone moieties (Aeschbacher et al., 2012; Ratasuk & Nanny, 2007; Uchimiya & Stone, 2009). Developing a conceptual understanding of these relations is therefore important to understand the mechanics of EAC_{POM} and EDC_{POM} changes during decomposition. Indicators of peat chemistry, for example, the N:C ratio (alternatively C:N; Biester et al., 2014), C_{OX}, and MIRS-derived humification indices (Broder et al., 2012) have been widely used to analyze the degree of decomposition of peat (Biester et al., 2014; Drollinger et al., 2020).

A practically useful product of such investigations may be the development of regression models to predict peat EAC_{POM} and EDC_{POM} from such indicators of peat chemistry or MIRS. For humic and fulvic acids, a close relation between the EAC and H:C ratio was found (Aeschbacher et al., 2010; Tan et al., 2017). MIRS has not yet

been used for the prediction of electrochemical properties of OM, but has proven useful for its qualitative analysis (Hernández-Montoya et al., 2012; Yuan et al., 2018) and the prediction of other peat properties (Artz et al., 2008). On the one hand, such regression models may enable inferring the EAC_{POM} and EDC_{POM} of peat samples from existing data, on the other hand, they may serve at least as qualitative and (particularly for MIRS-based models) fast and cost effective screening tools which could assist in mapping peat EAC_{POM} and EDC_{POM}.

To address these knowledge gaps, we investigated how peat chemistry relates to its EAC_{POM} and EDC_{POM}, and how decomposition may change both peat chemistry and its electrochemical properties. Moreover, we wanted to assess if peat EAC_{POM} and EDC_{POM} may be predicted from simple indicators of peat chemistry or MIRS. To this end, we aimed to (a) quantify under standardized conditions the EAC_{POM} and EDC_{POM} of peat material formed under various environmental conditions and with a range of degrees of decomposition, (b) analyze the relation of the EAC_{POM} and EDC_{POM} to bulk chemical properties, indicators for decomposition, and molecular structures, and (c) evaluate if element ratios (H:C, O:C, N:C, S:C) and MIRS can be used to predict peat EAC_{POM} and EDC_{POM}, all based on a global data set of peat materials.

These analyses represent a basis for the conceptual understanding of how peat chemistry and decomposition affect the EAC_{POM} and EDC_{POM}. This knowledge can help to understand, quantify, and predict spatiotemporal variability in peat EAC_{POM} and EDC_{POM} and thus contributes to the quantitative understanding of peatland decomposition processes and CH_4 formation on a global scale. With this, we aim to contribute information to better understand and predict peatland-climate interactions.

2. Materials and Methods

To answer our main research question—how peat chemistry relates to its EAC and EDC, and how decomposition may change both—we compiled peat material and data for peatland sites with a broad range of climate regimes, dominant vegetation, and peatland types and performed various measurements under standardized conditions to describe their chemical and electrochemical characteristics. With these data, we conducted an explorative analysis, computed regression models that predict the EAC_{POM} and EDC_{POM} from element ratios or MIRS, and finally developed a conceptual model how initial peat chemistry and decomposition change chemical characteristics and the EAC_{POM} and EDC_{POM} of peat.

2.1. Study Sites

We compiled peat cores collected in the course of different projects from 15 peatland sites (one core per site). The different peatland sites are spread across the range of mid to high-latitude peatland areas (Figure 1), experience different climatic regimes, and comprise both bogs and fens with different dominant vegetation cover (Table 1). This enabled us to analyze peat material with a representative range of chemical properties and EAC and EDC.

Peat samples were selected from four approximate depth levels, depending on the vertical resolution of the peat cores and the maximum depth reached during coring (10–20, 30–40, 60–70 cm, and the deepest available sample per core at depths of 140–320 cm). We assumed that the samples cover most of the decomposition and vegetation shift-related variability in peat chemistry and hence EAC and EDC.

2.2. EAC and EDC Measurements

We measured the EAC and EDC of the peat samples using mediated electrochemical reduction (MER) and oxidation (MEO), respectively, following largely the protocols provided by Lau et al. (2015) and Gao et al. (2019).

For this, the peat material was freeze dried (alpha 1–4 plus, Christ, Osterode, Germany) and finely ground to powder in a vibratory cup mill (tungsten carbide cups; Retsch MM 400, Haan, Germany). The ground samples were suspended in water in order to create a suspension that can be pipetted for analyses as described elsewhere (Lau et al., 2015). For this, approximately 0.08 g of sample and 30 mL of deionized, degassed, and anoxic water were used, or, in case of lower amounts of sample available, a similar ratio of water to solids. Aliquots of these bulk peat POM suspensions were used during the electrochemical measurements.

The suspensions were transferred into a glove box with N_2 atmosphere (<1 ppm O_2; Inert Lab Glovebox, Innovative Technology) to perform the electrochemical measurements. For each measurement, an aliquot of each

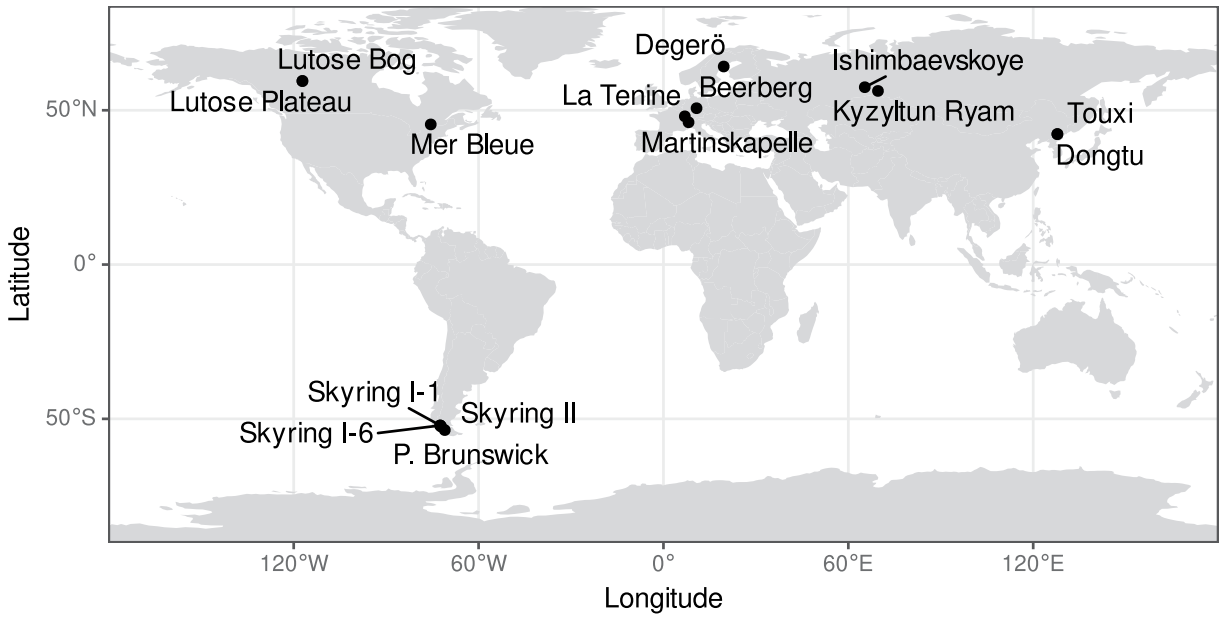

Figure 1. Map of the peatland sites from which peat material and data were compiled for this study. The map was created using data from the R package rnaturalearth (South, 2017).

Table 1
Overview on the Sites From Which Peat Samples and Data Were Derived From

Site label	Site name	Longitude	Latitude	Altitude	Peatland type	Current vegetation	Temperature	Precipitation	References
BB	Beerberg	10.74	50.66	977	Bog	*Sphagnum*, shrubs	5.3	1,349	
MK	Martinskapelle	8.15	46.10	2,089	Bog	Shrubs, *Sphagnum*	2.1	1,027	
LT	La Tenine	6.93	48.04	863	Bog	*Sphagnum*, shrubs	6.4	1,330	
DE	Degerö	19.56	64.18	275	Fen	*Sphagnum*, sedges, shrubs	1.7	621	Sagerfors et al. (2008)
ISH	Ishimbaevskoye	65.34	57.47	77	Fen	Shrubs, *Sphagnum*	1.5	472	Wertebach et al. (2016)
KR	Kyzyltun Ryam	69.62	56.26	110	Bog	*Sphagnum*	1.0	384	Larina et al. (2013)
TX	Touxi	127.84	42.28	1,070	Fen	Vascular plants, *Sphagnum*	1.3	754	
DT	Dongtu	127.86	42.27	1,268	Fen	Vascular plants, *Sphagnum*	0.6	775	
LB	Lutose Bog	−117.17	59.48	309	Bog	*Sphagnum*, shrubs	−1.8	356	Heffernan et al. (2020)
LP	Lutose Plateau	−117.17	59.48	309	Bog	*Sphagnum*, lichens	−1.8	356	Heffernan et al. (2020)
MB	Mer Bleue	−75.52	45.41	68	Bog	Shrubs, *Sphagnum*	5.6	945	Elliott et al. (2012)
PBR	P. Brunswick	−70.97	−53.64	50	Bog	*Sphagnum*, shrubs	6.0	797	Broder et al. (2012)
SKY I-1	Skyring I-1	−72.45	−52.14	75	Bog	Vascular plants (*Astelia pumila*), *Sphagnum*	6.1	637	Mathijssen et al. (2019)
SKY I-6	Skyring I-6	−72.45	−52.14	75	Bog	*Sphagnum*	6.1	637	Mathijssen et al. (2019
SKY II	Skyring II	−72.13	−52.51	36	Bog	*Sphagnum*	6.3	690	Broder et al. (2012)

Note. Longitude and latitude are given in decimal degree north and east, respectively (EPSG:3857), the altitude is given in meter above sea level, peatland type differentiates between bogs and fens following available studies for the respective sites or from own investigations following concepts in Rydin et al. (2013). "Temperature" is the mean annual temperature [°C], "Precipitation" is the total annual precipitation [mm], and "References" are references with additional information on the sites. Elevation data were derived from the median values of the GMTED2010 data (Danielson & Gesch, 2010). All climate data were derived from the WorldClim version 2.1 climate data for 1970–2000 (30 s spatial resolution, monthly temporal resolution) (Fick & Hijmans, 2017).

suspension, depending on the total organic carbon content and the expected range of the EAC/EDC (typically 100 µL suspension containing 0.13 ± 0.01 mg; the error refers to pipetting errors in the volume), was transferred into electrochemical cells. The suspensions were continuously stirred (topolino, IKA) to ensure reproducible transfer into the electrochemical cells.

The electrochemical cells and analytical setup consisted of a multichannel potentiostat (CH1000, CH Instruments), glassy carbon working electrodes (Sigradur, HTW), platinum counter electrodes (coiled 0.4 mm platinum wire, Sigma-Aldrich), and Ag/AgCl reference electrodes (RE-1B, ALS Co. Ltd). All potentials were experimentally measured against Ag/AgCl reference, but are reported versus the standard hydrogen electrode (MER: −0.49 V, MEO: 0.61 V).

The working electrode solution contained KCl as a background electrolyte (0.1 mol L^{-1}) and was buffered to pH 7 (0.2 mol L^{-1} KH_2PO_4) to ensure stable pH during measurements (Aeschbacher et al., 2011) and to enable direct comparisons with available data (Aeschbacher et al., 2010; Tan et al., 2017; Walpen, Getzinger, et al., 2018). Prior to analyses of samples 180 µL of a 0.1 mol L^{-1} solution of the mediator diquat (6,7-dihydrodipyrido [1,2-a:20,10-c] pyraziniumdibromid monohydrate; $EH_0 = -0.36$ V; Supelco, USA; 95% purity) was added for MER, and a similar amount of ABTS (2,2-azino-bis-(3-ethylbenzthiazoline-6-sulfonic acid) ammonium salt; $EH_0 = 0.68$ V; Sigma Aldrich, St. Louis, USA; 98% purity) for MEO.

Values of EAC and EDC were determined in MER and MEO, respectively, by integrating the reductive or oxidative current signals over time and normalizing the quantified numbers of electrons transferred to the amount of carbon added for analysis (Aeschbacher et al., 2010). The sum of EAC and EDC is referred to as total electron exchange capacity (EEC_{tot}).

In a strict sense, the obtained EAC and EDC values are the combined EAC and EDC of the POM, DOM, and dissolved inorganic ions and inorganic particles that could be reduced and oxidized, respectively. Prior studies of organic rich sediments and peat samples suggest that dissolved inorganic ions and DOM have a negligible contribution to the EAC and EDC of bulk peat material (∼1%; Gao et al., 2019; Lau et al., 2015) and therefore we assume that our measurements are representative for the solid phase.

Even though POM is assumed to be the dominant contributor to the EAC and EDC of organic rich sediments such as peat (Gao et al., 2019; Lau et al., 2015), solid iron phases can contribute to the EAC and EDC of peat as measured by MER/MEO (Lau et al., 2015). We therefore corrected the measured EAC and EDC values for contributions of Fe^{2+} (each mol contributing one mol electrons to the EDC) and Fe^{3+} (each mol contributing one mol electrons to the EAC; Gao et al., 2019; Lau et al., 2015). To this end, we extracted iron by adding 4 mL 1 mol L^{-1} HCl to 1 mL of each sample (in some cases less material had to be used), letting the suspensions rest for 72 hr in the dark, and filtering the solution through 0.22 µm Nylon syringe filters. Concentrations of Fe^{2+} and Fe^{3+} in the filtrate were measured spectrophotometrically using the 1,10-phenanthroline method (Tamura et al., 1974) and from this, we computed the contributions of iron to the EAC ($EAC_{Fe}{}^{3+}$) and EDC ($EDC_{Fe}{}^{2+}$), respectively. The EAC_{POM} was then computed by subtracting $EAC_{Fe}{}^{3+}$ from the measured EAC and the EDC_{POM} by subtracting $EDC_{Fe}{}^{2+}$ from the measured EDC (Lau et al., 2015).

There are several known issues with this procedure. First, acid extraction may not extract all redox active iron moieties (Lau et al., 2016). Second, during acid extraction, the redox equilibrium between iron and OM is shifted and Fe^{3+} may in part be reduced to Fe^{2+} (Lau et al., 2015). Consequently, the contribution of iron to the EDC is typically overestimated, whereas the contribution of iron to the EAC is typically underestimated (Lau et al., 2015).

The first issue may be negligible for most samples because peat typically contains few mineral particles and hence most iron typically is acid extractable (Figure S3 in Supporting Information S1). However, we cannot fully exclude that more iron moieties than that accessible via acid extraction contributed to the EAC and EDC for samples with larger iron contents (Figure S3 in Supporting Information S1). The second issue probably affected our calculated EAC_{POM} and EDC_{POM} values. One indication for this is that 5 EDC_{POM} values were negative (minimum: −8 µmol g_C^{-1}). We therefore assume that the calculated EAC_{POM} and EDC_{POM} values are biased for samples with high iron content and considered this during data analysis and interpretation (see below).

We finally report the EAC_{POM} and EDC_{POM} relative to the C mass of the measured sample (mass of C in the bulk peat POM suspension aliquot). Moreover, we computed the EAC_{POM} and EDC_{POM} relative to the total mass of the

sample for comparison with values reported in other studies. For each sample, we computed average EAC_{POM} and EDC_{POM} values and respective standard deviations from the replicate measurements. During this, we discarded one EAC replicate measurement for which we assumed measurement errors because it differed extremely (more than 1,000 μmol g_C^{-1}) from the remaining replicate measurements for the same sample (Figure S2 in Supporting Information S1).

The EAC_{POM} and EDC_{POM} values we report here can be interpreted as material properties because all measurements have been standardized to specific conditions (pH value, oxidation state of the POM, reduction potentials, ionic strength of the solution, standardized particle size due to milling; Aeschbacher et al., 2012; Lu et al., 2015). This is necessary to interpret the EAC_{POM} and EDC_{POM} values relative to the chemistry of the POM because otherwise the measured EAC_{POM} and EDC_{POM} values would be confounded by factors not related to the chemistry and degree of decomposition of the peat POM. The values measured in this study therefore probably differ from EAC_{POM} and EDC_{POM} values under in situ conditions due to different environmental conditions and intact physical structure of the peat POM. Due to an intact physical structure and more acidic conditions, in situ EAC_{POM} and EDC_{POM} probably are smaller than the values reported here (Aeschbacher et al., 2012; Lu et al., 2015). If electron transfer within intact POM over larger distances occurs (Bai et al., 2020), smaller EAC_{POM} and EDC_{POM} values under the same pH value and ionic strength would probably be a result of kinetic limitation and therefore longer measurements may be necessary to fully oxidize/reduce redox active moieties. Comparative values measured under in situ conditions are yet not available because it is currently practically difficult to measure the EAC and EDC under in situ conditions.

2.3. Element Contents

We analyzed concentrations of C, N, and S for all samples by catalytic combustion using an elemental analyzer (EA 3000, Eurovector). Concentrations of H and O were determined based on the modified Dumas Method, using a CHNS/O analyzer (FlashEA 1,112, Thermo Fisher Scientific). The nominal oxidation state of C (C_{ox}) was computed from the contents of C, H, N, and O (Masiello et al., 2008; Worrall et al., 2016).

Total concentrations of other elements (Fe, P and others; see Table S1 in Supporting Information S1 for a full list of measured elements) were determined by wavelength dispersive X-ray fluorescence spectroscopy (WD-XRF; ZSX Primus II) calibrated with a set of 15 reference materials, consisting of certified plant, peat, and sediment materials, and 5 in-house working standards. Analyses were done on 500 mg of ground, powdered sample, pressed to a 13 mm pellet (without pelleting aids) at a load of approximately 7t. For few samples, S contents were derived from the WD-XRF data.

2.4. Mid Infrared Spectroscopy

Fourier-transform mid infrared spectra (MIRS) were used to obtain detailed information on peat molecular structures and to compute regression models for the prediction of peat EAC and EDC. Two mg of powdered sample were mixed with 200 mg KBr (FTIR grade, Sigma Aldrich) and pressed to a 13 mm pellet. Spectra were recorded on a Cary 660 FTIR spectrometer (Agilent) in the range 650–4,000 cm^{-1} at a resolution of 0.5–2 cm^{-1}. A number of 32 scans per sample was collected in absorbance mode and a KBr background was subtracted.

The recorded MIRS were preprocessed to remove known artifacts and harmonize the data. Spectral preprocessing was performed using the package ir (0.0.0.9000; Teickner, 2021). To assess the degree of peat decomposition, we computed a humification index by dividing the intensity at 1,630 cm^{-1} and 1,090 cm^{-1} (denoted as $HI_{1630/1090}$; Broder et al., 2012) using irpeat (0.0.0.9000; Teickner & Hodgkins, 2021).

Two transformed versions of the spectra were created for the computation of MIRS-based regression models: The first is a binned version and the second is a derived and binned version of the preprocessed spectra. Binning was performed with a bin width of 10 cm^{-1} to reduce autocorrelation and noise in the spectra. Prior to binning, the preprocessed spectra were derived using a Savitzgy-Golay filter (filter width: 5 cm^{-1}; signal developers, 2014). Derivatization can improve the resolution of features and therefore can improve the predictive accuracy of regression models (Engel et al., 2013; Stuart, 2004).

2.5. Statistical Analyses

2.5.1. Balancing the Analytical Bias in EAC_{POM} and EDC_{POM} Values

As mentioned in the previous section, the EAC_{POM} and EDC_{POM} values computed from measured EAC and EDC values and acid extracted iron ion contents probably are biased, especially for samples with high iron content (Lau et al., 2015, 2016). Since we are interested in electrochemical properties of POM, this bias must be considered during all data analysis steps. We aimed to do this first by quantifying the maximum potential contribution of iron to the EAC and EDC, second, by creating a filtered data set for each the EAC_{POM} and EDC_{POM} containing only data where the maximum potential contribution of iron to either the EAC and EDC was $\leq$100 μmol g_C^{-1}, and third, performing all analyses for the filtered data set. Analyses for the unfiltered data set can be found in Supporting Information S1.

The maximum potential contribution of iron to the EAC and EDC was determined as the total concentration of iron in the acid extract (sum of the concentrations of Fe^{2+} and Fe^{3+}). We assumed that non-extracted iron is redox inactive and hence this total iron concentration reflects the maximum potential contribution of iron to either the EAC or EDC, irrespective of the initial redox state and redox state changes during the acid extraction. This assumption is true for samples with low total iron contents, but cannot be validated for samples with larger iron contents (Figure S3 in Supporting Information S1; Lau et al., 2016). An overview on the maximum potential contribution of iron to the EAC and EDC across all samples computed from the acid extractable iron content can be found in Figure S4 in Supporting Information S1. The threshold of $\leq$100 μmol g_C^{-1} was chosen to balance the reduction in the analytical bias in the filtered data and the reduction in sample size, resulting in a sample size of 52 for the EAC and EDC. As a result, there was only a constant offset bias between corrected and uncorrected values for the EAC and EDC (Figure S5 in Supporting Information S1).

In general, measured EAC and EDC values typically are much larger than 100 μmol g_C^{-1} and samples with large acid extracted (and total) iron contents typically have a small EAC and EDC (Figures S5 and S6 in Supporting Information S1), suggesting that the maximum bias is probably low. Therefore we assume that it is unlikely that the remaining bias had a large influence on the results. As mentioned above, we cannot, however, fully exclude contributions of non-acid extractable iron minerals to the EAC and EDC. We also note that choosing a tighter filter threshold is likely to cause selection bias since samples with high acid extracted iron content tend to be more decomposed (Figure S7 in Supporting Information S1).

2.5.2. EAC_{POM} and EDC_{POM} Variability

We created several plots and computed Pearson correlation coefficients to analyze patterns in the samples' EAC_{POM} and EDC_{POM}. In particular, we compared our EAC_{POM} and EDC_{POM} values with those measured for various humic and fulvic acids and DOM samples in other studies (Aeschbacher et al., 2012; Tan et al., 2017; Walpen, Getzinger, et al., 2018). These values from other studies were extracted from the publications' figures using the R package digitize (Poisot, 2011).

2.5.3. Relation to Chemical Properties, Decomposition Indicators, and Infrared Spectra

To analyze the relation of the EAC_{POM}, EDC_{POM}, and EDC_{POM}:EAC_{POM} ratio to different indicators of bulk peat chemistry (H:C, O:C, N:C, S:C ratio, $HI_{1630/1090}$, and C_{OX}), we created scatterplots and computed their pairwise Pearson correlation (ρ). The H:C ratio has been shown to relate negatively to the EAC and EDC of humic and fulvic acids (Aeschbacher et al., 2010; Lv et al., 2018; Tan et al., 2017). The O:C, N:C, S:C ratio, and C_{OX} are indicators for peat decomposition (Biester et al., 2014; Leifeld et al., 2012; Masiello et al., 2008) and C_{OX} was positively related to the EDC of humic and fulvic acids (Lv et al., 2018). The O:C ratio is an indicator for the amount of polysaccharides (Kim et al., 2003) which are not assumed to contribute to the EAC_{POM} and EDC_{POM}. There is some evidence for the contribution of nitrogen and sulfur containing functional groups to the EAC_{POM} and EDC_{POM} (Fimmen et al., 2007; Hernández-Montoya et al., 2012; Ratasuk & Nanny, 2007) and the N:C, and S:C ratio might give information on this, too.

To qualitatively analyze potential joint effects of the H:C and O:C ratio and relate their variability to different OM fractions, we created van-Krevelen plots. For some International Humic Substances Society (IHSS) reference humic and fulvic acids (terrestrial and aquatic), information on element contents (Huffman Laboratories & Soil Biochemistry Laboratory University of Minnesota, NA) and EAC and EDC (Aeschbacher et al., 2012) are available. We therefore could include these samples in the van-Krevelen plots. Finally, we computed correlation

spectra for the EAC_{POM} and EDC_{POM} by computing the Pearson correlation of both variables with each MIRS variable. This allowed us to investigate relations to molecular structures derived from MIRS.

2.5.4. Regression Models

We used regression models to analyze if peat EAC_{POM} and EDC_{POM} can be predicted from a linear combination of individual element ratios (H:C, O:C, N:C, S:C). Different regression approaches were investigated: (a) including only the H:C and O:C ratio, and (b) including all four element ratios. We used Bayesian hierarchical models to consider the uncertainties of the replicate measurements and that these were different for different samples (Figure S8 in Supporting Information S1 provides an overview on the model structure). For the EAC_{POM} and EDC_{POM} values (both individual measurements and replicate measurement averages), we assumed a Gamma distribution with log-link function. Individual replicate measurements with EDC_{POM} values ≤ 0 μmol g_C^{-1} were set to 0 μmol g_C^{-1} for this. Since the absolute values of these measurements is small in comparison to the median EDC_{POM} values, we assumed that this causes no bias in our analyses. Further details on the specification of the element ratio-based models can be found in Supporting Information S1.

Additionally, we computed regression models to analyze the joint relation of molecular structures derived from MIRS to the EAC_{POM} and EDC_{POM}. For this, we used partial least squares regression (PLSR) and Bayesian regularization (e.g., Artz et al., 2008; Ferragina et al., 2015). Since different preprocessing approaches for MIRS can affect the predictive performance of models (Engel et al., 2013), we computed not only one regression model for each the EAC_{POM} and EDC_{POM}, but four, using either non-derived spectra or first derivative spectra as input data, and PLSR or Bayesian regularization, respectively. In addition, for the EDC_{POM}, we observed biases and tried to reduce these by dividing the EDC_{POM} by $HI_{1630/1090}$.

We applied Bayesian projection (Piironen et al., 2020) on all MIRS-based models to facilitate their interpretation. Bayesian projection seeks to find a reduced model that is similar to the full model in terms of its posterior distribution within some defined tolerance threshold (Piironen et al., 2020). This allowed us to establish more direct links between the underlying molecular structures and the EAC_{POM} and EDC_{POM}. Further details on the projection approach are described in in Supporting Information S1.

We also wanted to analyze if regression models using element ratios or mid infrared variables may be used to predict peat EAC_{POM} and EDC_{POM}. For this, we estimated the predictive accuracy using 10-fold cross-validation (CV; Roberts et al., 2017) and the root mean square error (RMSE) as performance metric (Bellocchi et al., 2010). As we did not observe large deviations between alternative regression models, we cross-validated only the regression models containing all element ratios (H:C, O:C, N:C, S:C) and the MIRS-based models using Bayesian regularization and non-derived spectra. The RMSE was computed between the Markov Chain Monte Carlo (MCMC) draws for predictions of the regression models for new observations and MCMC draws for estimates of the samples' average EAC_{POM} or EDC_{POM}, respectively. This allowed us to consider the uncertainties of the repeated measurements during CV, and to compute a probability distribution for the RMSE values based on the CV uncertainty, as well as the models' uncertainties.

3. Results

3.1. EAC_{POM} and EDC_{POM}

Our peat samples' average EAC_{POM} ranges between 179 and 1,228 μmol g_C^{-1} and their EDC_{POM} between 9 and 569 μmol g_C^{-1} (after filtering; see Table 2 for site-specific values). The EAC_{POM} is typically larger than the EDC_{POM}, with few exceptions, and both are loosely positively related ($\rho = 0.39$), as shown in Figure 2b.

The EAC_{POM} and EDC_{POM} vary considerably between different sites and the depth-related within-site variability is also large (Figure 2a). In addition, no general depth-related pattern is visible: For some peat cores, the uppermost sample had the largest EAC_{POM} or EDC_{POM}, for others the deepest, and for some the intermediate samples. The same figure also shows that the EAC_{POM} and EDC_{POM} can change independently or even inversely to each other along the peat profile. Finally, our specific sites did not show distinct patterns in their EAC_{POM} and EDC_{POM} to differentiate bogs and fens (Figure S10 in Supporting Information S1).

Figure 2c compares EAC_{POM} and EDC_{POM} for our peat samples to those for different humic and fulvic acids and peat DOM samples obtained from different studies (Aeschbacher et al., 2012; Tan et al., 2017; Walpen, Getzinger,

Table 2
Overview on the Electrochemical and Chemical Properties and Decomposition States of the Peat Samples for the Different Sites (Mean, Min, Max)

Site label	EAC_{POM}	EDC_{POM}	H:C	O:C	N:C	S:C	C_{OX}	$HI_{1630/1090}$
BB	477 (390, 534)	397 (327, 463)	1.46 (1.4, 1.5)	0.68 (0.62, 0.74)	0.01 (0.01, 0.02)	0.001 (0, 0.003)	−0.07 (−0.12, 0.02)	0.56 (0.44, 0.62)
MK	581 (339, 940)	341 (213, 492)	1.44 (1.43, 1.45)	0.61 (0.52, 0.69)	0.02 (0.01, 0.03)	0.001 (0, 0.001)	−0.16 (−0.29, −0.01)	0.72 (0.55, 0.86)
LT	542 (427, 734)	310 (161, 452)	1.49 (1.48, 1.52)	0.68 (0.66, 0.7)	0.01 (0.01, 0.02)	0.001 (0, 0.001)	−0.1 (−0.13, −0.05)	0.58 (0.5, 0.63)
DE	477 (424, 590)	466 (288, 673)	1.55 (1.49, 1.61)	0.66 (0.6, 0.7)	0.02 (0.01, 0.02)	0 (0, 0.001)	−0.18 (−0.25, −0.08)	0.54 (0.49, 0.59)
ISH	633 (435, 926)	227 (176, 349)	1.42 (1.35, 1.48)	0.57 (0.54, 0.61)	0.02 (0.02, 0.03)	0.001 (0.001, 0.003)	−0.22 (−0.28, −0.13)	0.93 (0.66, 1.1)
KR	721 (486, 907)	402 (276, 548)	1.5 (1.39, 1.56)	0.65 (0.59, 0.69)	0.02 (0.01, 0.02)	0.001 (0.001, 0.001)	−0.16 (−0.25, −0.09)	0.75 (0.64, 1.01)
TX	415 (302, 636)	80 (36, 128)	1.51 (1.47, 1.56)	0.56 (0.53, 0.61)	0.04 (0.04, 0.05)	0.002 (0.001, 0.002)	−0.27 (−0.31, −0.2)	0.83 (0.61, 0.98)
DT	325 (255, 388)	121 (98, 140)	1.47 (1.4, 1.53)	0.5 (0.48, 0.53)	0.04 (0.04, 0.05)	0.002 (0.001, 0.002)	−0.33 (−0.38, −0.31)	0.89 (0.8, 0.99)
LB	642 (324, 1,208)	363 (284, 410)	1.48 (1.29, 1.63)	0.68 (0.57, 0.73)	0.02 (0.01, 0.02)	0.001 (0, 0.002)	−0.06 (−0.13, −0.01)	0.45 (0.37, 0.62)
LP	968 (691, 1,228)	269 (207, 334)	1.4 (1.28, 1.54)	0.65 (0.6, 0.7)	0.02 (0.01, 0.02)	0.001 (0, 0.001)	−0.04 (−0.08, 0)	0.61 (0.55, 0.66)
MB	758 (656, 868)	351 (247, 569)	1.41 (1.31, 1.46)	0.64 (0.52, 0.72)	0.02 (0.01, 0.03)	0.001 (0, 0.001)	−0.09 (−0.21, 0.05)	0.69 (0.47, 0.95)
PBR	799 (455, 1,192)	461 (376, 541)	1.38 (1.3, 1.45)	0.6 (0.56, 0.65)	0.02 (0.01, 0.02)	0.001 (0.001, 0.001)	−0.12 (−0.15, −0.11)	0.83 (0.7, 0.95)
SKY I-1	323 (179, 468)	76 (10, 155)	1.43 (1.38, 1.51)	0.58 (0.55, 0.63)	0.03 (0.02, 0.04)	0 (0, 0.001)	−0.2 (−0.29, −0.07)	0.9 (0.54, 1.13)
SKY I-6	346 (234, 497)	169 (58, 269)	1.44 (1.4, 1.48)	0.55 (0.48, 0.62)	0.02 (0.02, 0.02)	0 (0, 0.001)	−0.28 (−0.38, −0.14)	0.92 (0.65, 1.37)
SKY II	749 (570, 912)	376 (347, 403)	1.46 (1.44, 1.48)	0.67 (0.53, 0.74)	0.01 (0.01, 0.02)	0 (0, 0.001)	−0.07 (−0.32, 0.08)	0.58 (0.44, 0.73)

Note. EAC_{POM} and EDC_{POM} are given in μmol g_C^{-1}. element ratios are molar ratios. C_{OX} is the nominal oxidation state of carbon. $HI_{1630/1090}$ is the ratio of the intensities at 1,630 and 1,090 cm^{-1} computed from mid infrared spectra.

et al., 2018). Most humic and fulvic acids and peat DOM samples have a larger EAC and EDC on a per gram carbon scale, whereby mineral soil humic and fulvic acids (Tan et al., 2017) seem to have intermediate values relative to our measurements on the one hand and the larger values for various IHSS reference samples (Aeschbacher et al., 2012) and peat DOM samples (Walpen, Getzinger, et al., 2018) on the other hand.

3.2. Relation to Bulk Chemical Properties

No single bulk chemical property is strongly related to either the EAC_{POM}, EDC_{POM} or EDC_{POM}:EAC_{POM} ratio, except for the N:C ratio which is relatively strongly related to the EDC_{POM} ($\rho = -0.65$), and the H:C ratio which is related to the EAC_{POM} ($\rho = -0.47$; Figure S11 in Supporting Information S1). The EDC_{POM}:EAC_{POM} ratio is related to the N:C ratio ($\rho = -0.5$). All other Pearson correlation coefficients between either the EAC_{POM} or EDC_{POM} and any of the variables we considered is not larger than 0.45 or smaller than −0.43.

The relative weak correlations are not due to non-linear relations, but due to a large variability within and between sites (Figure S11 in Supporting Information S1). For the EAC_{POM}, this variability is especially large for samples with average N:C ratio, medium to large O:C ratio, large C_{OX}, and medium $HI_{1630/1090}$. For the EDC_{POM},

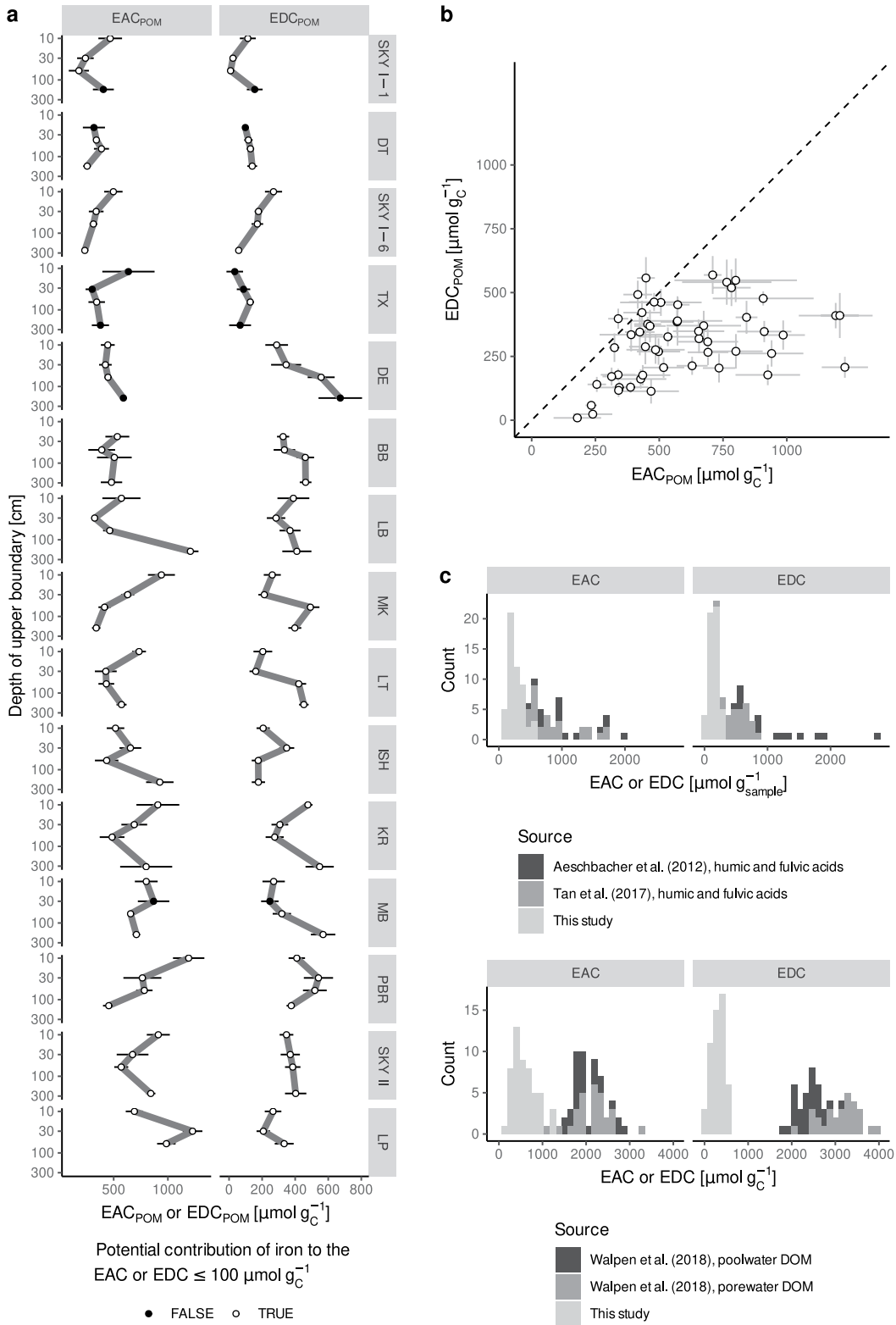
a
EAC_POM
EDC_POM
SKY I−1
DT
SKY I−6
TX
DE
BB
LB
MK
LT
ISH
KR
MB
PBR
SKY II
LP
Depth of upper boundary [cm]
10
30
100
300
500
1000
0
200
400
600
800
EAC_POM or EDC_POM [µmol g_C^-1]
Potential contribution of iron to the EAC or EDC ≤ 100 µmol g_C^-1
FALSE
TRUE
b
EDC_POM [µmol g_C^-1]
EAC_POM [µmol g_C^-1]
0
250
500
750
1000
c
EAC
EDC
Count
EAC or EDC [µmol g_sample^-1]
Source
Aeschbacher et al. (2012), humic and fulvic acids
Tan et al. (2017), humic and fulvic acids
This study
EAC or EDC [µmol g_C^-1]
Walpen et al. (2018), poolwater DOM
Walpen et al. (2018), porewater DOM
This study

Figure 2.

the variability is large for medium to small O:C ratio, medium to small C_{OX}, and medium $HI_{1630/1090}$. For the EDC_{POM}:EAC_{POM} ratio, the variability is large for small to medium N:C ratios and $HI_{1630/1090}$.

EAC_{POM} and EDC_{POM} values are large along a gradient with large O:C and large H:C ratio at the one end and small O:C and small H:C ratio at the other end (Figure 3). Conversely, samples with small O:C ratio, but large H:C ratio have the smallest EAC_{POM} and EDC_{POM}. Whilst this gradient is a general pattern, there are some samples with smaller and larger EAC_{POM} and EDC_{POM} values than could be expected based on the described gradient. For instance the two samples from SKY I-1 at intermediate depth have a surprisingly small EAC_{POM} and EDC_{POM}, and samples from SKY II and Martinskapelle (MK) have a large EAC_{POM} and EDC_{POM} for their small O:C and large H:C ratio (Figure 3).

To compare these patterns to those for humic and fulvic acids, we present the same variables in Figure 3b, but including various IHSS reference humic and fulvic acids and measured EAC and EDC values from Aeschbacher et al. (2012) for some of these. The H:C values of the humic and fulvic acids are separated by ∼0.5 from that of the peat samples, whereas there is a rather large overlap in the O:C ratio between both sample groups. One exception is the Pony Lake FA which has a H:C ratio similar to our peat samples. Overall, the humic and FA samples, with their larger EAC and EDC, extent the gradient we observed for the peat samples. We additionally labeled regions according to OM fractions typically delineated in van-Krevelen diagrams (Kim et al., 2003). The peat samples spread between the cellulose and lignin regions, whereas the humic and FA samples are shifted more towards the lignin region due to their small H:C ratios (except Pony Lake FA; Figure 3b).

This observed gradient is partly also supported by the regression models. For the EAC_{POM}, the H:C ratio has a negative coefficient ($\beta_{H:C} \in [-2.58, -0.8]$; All reported intervals are 95%-posterior intervals for the models with all element ratios and Gaussian coefficients, except if stated differently) and the O:C ratio a positive coefficient ($\beta_{O:C} \in [0.38, 2.27]$) for all models. For the EDC_{POM}, the O:C ratio only has a positive coefficient ($\beta_{O:C} \in [0.7, 1.92]$) if the N:C and S:C ratio are not included, whereas the coefficients' posterior intervals for the H:C ratio broadly overlaps zero ($\beta_{H:C} \in [-1.09, 0.37]$). If the N:C and S:C ratio are included in the model, the coefficient for the O:C ratio ($\beta_{O:C} \in [-0.64, 1.09]$) and H:C ratio ($\beta_{H:C} \in [-0.54, 0.93]$) clearly overlap zero.

For the EAC_{POM}, neither the N:C ($\beta_{N:C} \in [-0.82, 0.86]$), nor the S:C ratio ($\beta_{S:C} \in [-0.17, 0.74]$) have a clearly from zero different coefficient. For the EDC_{POM}, the S:C ratio is also not clearly different from zero ($\beta_{S:C} \in [-0.32, 0.7]$), whereas the model implies a negative relation for the N:C ratio ($\beta_{N:C} \in [-2.55, -0.63]$). Thus, it seems that the EAC_{POM} is linearly mainly related to the H:C and O:C ratio, whereas the EDC_{POM} is mainly related to the N:C ratio.

3.3. Relation to Molecular Structures

MIR variables typically assigned to labile OM fractions tend to be positively related to the EAC_{POM} and EDC_{POM} and variables typically assigned to more recalcitrant OM fractions tend to be negatively related to the EAC_{POM} and EDC_{POM} (Figure S12 in Supporting Information S1). This is evident from positive correlations with MIR variables representing cellulose C-O stretching, phenol C-O stretching and O-H bending, carbonyl C=O stretching, cellulose and phenol O-H stretching and negative correlations with MIR variables representing aromatic C=C stretching, C-H bending, and lipid C-H stretching (Artz et al., 2008; Cocozza et al., 2003; Kubo & Kadla, 2005; Schmidt et al., 2006; Stuart, 2004). However, the correlations are overall relatively small (maximum absolute correlation = 0.61).

The general patterns in the correlation spectra for the EAC_{POM} are similar to those for the EDC_{POM}. Some deviations are visible: For example, the EDC_{POM} has a more negative relation to aromatic C=C stretching, and a more

Figure 2. (a) Depth profiles of the EAC_{POM} and EDC_{POM} for each peat core. Thick curves represent the median values of the replicate measurements and horizontal lines the standard error of the replicate measurements. Sites are sorted according to their median EAC_{POM}. The depth is presented log-scaled. Different colors indicate samples for which the potential maximum contribution of iron to the EAC or EDC is larger than 100 μmol g_C^{-1} (b) Plot of the average EAC_{POM} versus the average EDC_{POM}. Error bars represent the respective standard errors from replicate measurements. Samples below the diagonal line have a larger EAC_{POM} than EDC_{POM}. Only samples with a potential contribution of iron to the EAC and EDC ≤100 μmol g_C^{-1} are shown. (c) Histograms of the EAC and EDC values, respectively, for the peat POM samples analyzed in this study, humic and fulvic acids, and DOM analyzed in other studies. Top: Values reported in μmol g_{sample}^{-1}. Bottom: Values reported in μmol g_C^{-1}. Only samples with a potential contribution of iron to the EAC and EDC ≤100 μmol g_C^{-1} are shown.

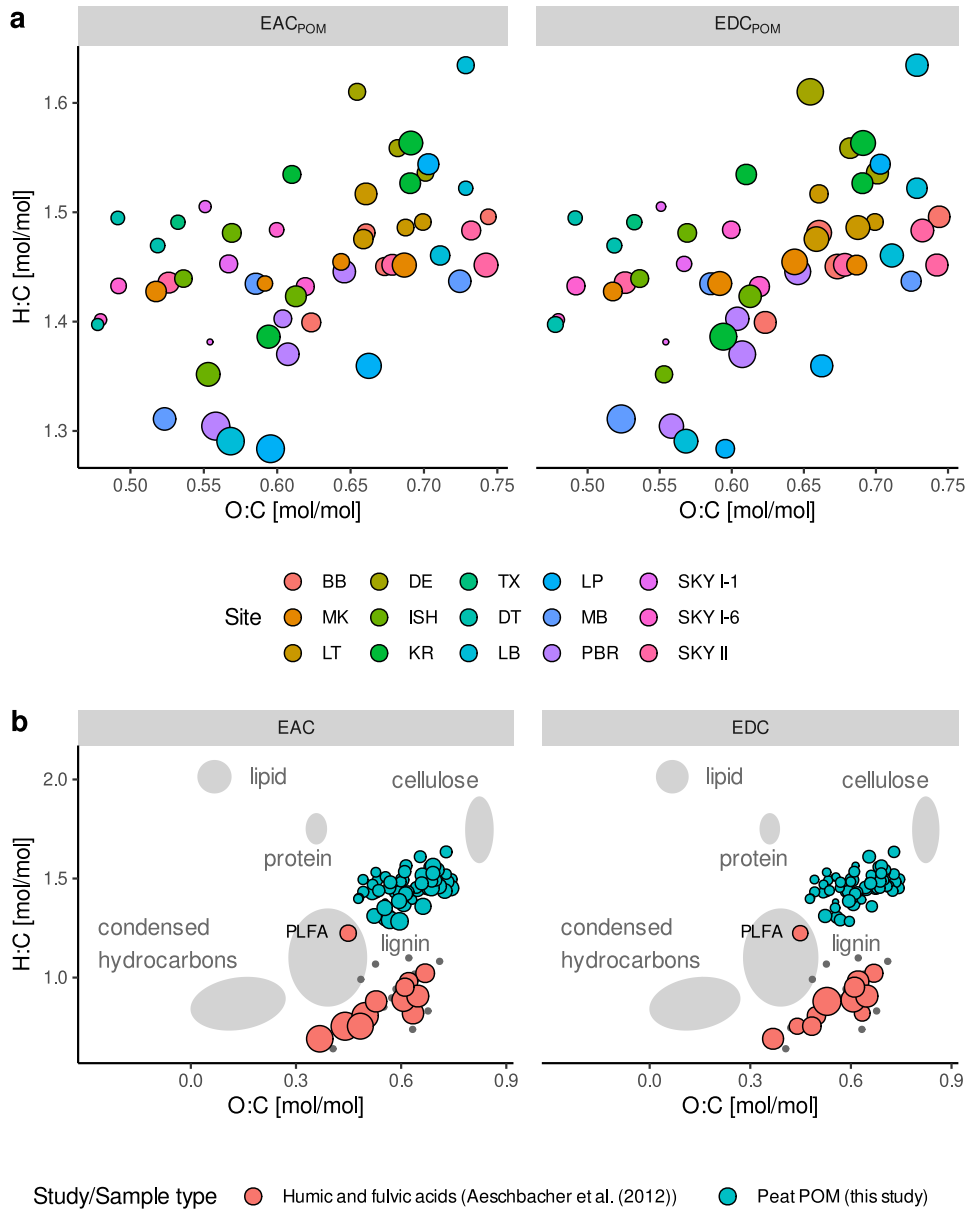

Figure 3. Van-Krevelen-like plot for the peat samples analyzed in this study. (a) Points are scaled relative to the EAC and EDC, respectively, and colored accoring to the sites the samples were taken from. (b) The same as a, but including all samples from this study and various IHSS reference humic substances (red and small gray points) in addition to our peat samples (blue points). Humic and fulvic acids for which Aeschbacher et al. (2012) measured EAC and EDC data are filled red and scaled according to these values. Humic and fulvic acids for which this was not the case are represented as uniformly small gray points. Moreover, we highlighted regions commonly attributed to different OM fractions in van-Krevelen plots (Kim et al., 2003). PLFA is the Pony Lake FA reference material. From this study, only samples with a potential contribution of iron to the EAC and EDC ≤100 μmol g_C^{-1} are shown and point sizes are scaled relative to the EAC$_{POM}$ and EDC$_{POM}$, respectively.

positive relation to cellulose and phenol O-H stretching, whereas the EAC$_{POM}$ is more strongly related to carbonyl C=O stretching.

Variable selection during the regression analysis identified 6 and 2 variables as sufficient to predict the EAC$_{POM}$ and EDC$_{POM}$, respectively: The EAC$_{POM}$ is positively related to carbonyl group C=O stretching and tends to be negatively related to lipid C-H stretching, O-H stretching of unbonded OH groups, and C-H bending of (potentially polysubstituted) aromatics (Table 3). For lipid C-H stretching and unbonded O-H stretching, two directly

Table 3
Assignment of MIR Variables Included in the Projected Regression Models for the EAC_{POM} and EDC_{POM} Using the Filtered Data Set, Respectively

Wavenumber	Coefficient		Assigned structure	Reference
	EAC_{POM}	EDC_{POM}		
830	−0.13 (−0.28, 0.03)		C-H bending of di- or trisubstituted aromatics	Stuart (2004)
1,530		−0.23 (−0.68,0.17)	Secondary amide N-H bending and C-N stretching	Stuart (2004)
1,720	0.41 (0.19, 0.62)		Carbonyl C=O stretching (carboxyls, esters, ketones - aliphatic and aromatic)	Cocozza et al. (2003), Stuart (2004), Artz et al. (2008)
2,890	−0.71 (−1.1, −0.28)		Lipid C-H stretching	Cocozza et al. (2003), Stuart (2004), Artz et al. (2008)
2,910	0.1 (−0.27, 0.45)		Lipid C-H stretching	Cocozza et al. (2003), Stuart (2004), Artz et al. (2008)
3370		0.34 (−0.09,0.75)	O-H stretching of bonded OH groups (cellulose, phenols)	Stuart (2004), Kubo and Kadla (2005) Schmidt et al. (2006)
3660	1.45 (−0.84, 3.58)		O-H stretching of unbonded OH groups	Stuart (2004), Kubo and Kadla (2005) Schmidt et al. (2006)
3670	−1.88 (−4.02, 0.42)		O-H stretching of unbonded OH groups	Stuart (2004), Kubo and Kadla (2005) Schmidt et al. (2006)

Note. "Wavenumber" represents the average bin position wavenumber value of the mir variable that were selected. "Coefficient" are the estimated coefficients for the variables (mean and limits of the 95% posterior intervals).

neighboring variables with partly contrasting coefficients (positive and negative) were selected. However, their joint relation to the EAC_{POM} is clearly negative (Figure S19 in Supporting Information S1). The EDC_{POM} tends to be positively related to O-H stretching of intramolecularly bonded OH groups, probably of cellulose and phenols, and tends to be negatively related to secondary amide N-H bending and C-N stretching (Table 3).

Overall, this indicates that the EAC_{POM} is positively related to carbonyl groups and negatively related to structures more abundant in decomposed peat (lipids, aromatics, unbonded OH groups), and the EDC_{POM} is positively related to structures more abundant in undecomposed peat (intramolecular OH bonds in cellulose and phenols).

3.4. Predictive Accuracy of the MIRS-Based Models in Comparison to Regression Models Based on Element Ratios

The predictive performances of the different modeling approaches (MIRS-based vs. element ratio-based) do not differ considerably, and their respective CV-RMSEs are several times larger than the standard deviation of the distributions for the respective replicate measurements. The MIRS-based models had a median 10-fold CV-RMSE 23.5 and 4.4 μmol g_C^{-1} smaller and larger than the element ratio-based models for the EAC_{POM} and EDC_{POM}, respectively. The models with the least median 10-fold CV-RMSE for each variable had a 10-fold CV-RMSE of 250.4 [101.3, 509] and 160.5 [58.1, 279.7] μmol g_C^{-1} for the EAC_{POM} and EDC_{POM}, respectively. In comparison to this, the median standard deviation from the estimated distribution for the measured values is 36.2 and 21.2 μmol g_C^{-1}. In spite of the similar predictive performance of both models for the EAC_{POM}, the MIRS-based model is clearly less biased than the element ratio-based model, whereas both models for the EDC_{POM} are clearly biased (Figure S15 in Supporting Information S1).

Using derivative spectra, data subsets, or PLSR instead of Bayesian regularization neither yield considerably worse, nor better models in terms of their training predictive accuracy (Figure S18 in Supporting Information S1).

4. Discussion

To answer how peat chemistry relates to its EAC_{POM} and EDC_{POM} and how decomposition changes both, we use our results to develop a conceptual model describing how vegetation chemistry and intensity of aerobic decomposition control peat electrochemical properties via the amount of polymeric phenols and quinones.

The analyzed peat samples cover a globally representative range of mid to high latitude peat properties and degrees of decomposition (Table 2). The element ratio data are within the ranges reported by several larger

compilations of peat chemical properties (Moore et al., 2018; Leifeld et al., 2020; M. Wang et al., 2015; Loisel et al., 2014; Tipping et al., 2016). The same is true for C_{OX} values (Leifeld et al., 2020; Moore et al., 2018; Worrall et al., 2016). Overall, we are confident that our findings and interpretations should hold for a broad range of peat materials and thus are generalizable.

4.1. Quinones and Phenols Are Main Contributors to Peat EAC_{POM} and EDC_{POM}

Our results point towards quinones and phenols as main contributors to the EAC_{POM} and EDC_{POM} of peat, respectively. EAC_{POM} and EDC_{POM} values are large along a H:C-O:C gradient with large O:C and large H:C ratio at the one end and small O:C and small H:C ratio at the other end (Figure 3). Based on commonly delineated H:C-O:C regions in van-Krevelen diagrams (Kim et al., 2003), we assume that this gradient characterizes material rich in polymeric quinones and phenols. This interpretation is also supported by the positive relation to carbonyl groups which are characteristic for polymeric quinones and phenols (El Mansouri & Salvadó, 2007; Figure S12 in Supporting Information S1). In addition, the more pronounced negative correlation of the EDC_{POM} to the N:C ratio in comparison to the EAC_{POM} can be explained with the larger susceptibility of phenols towards decomposition in contrast to quinones which are formed by partial oxidation of phenols (Aeschbacher et al., 2012; Bolton et al., 2018; Fenner & Freeman, 2011). We expected this finding since quinones and phenols have been identified as major contributors to OM EAC and EDC in general (Aeschbacher et al., 2010, 2012; Ratasuk & Nanny, 2007).

We did not find clear relations of the N:C or S:C ratio to the EAC_{POM} and EDC_{POM} that would point towards a large contribution of non-quinone moieties to the EAC_{POM} or EDC_{POM}. In fact, the N:C ratio is negatively related to the EDC. A small non-quinone EAC and EDC is in line with the relative small S and N contents of the peat samples and the neutral pH value our measurements were standardized to (Fimmen et al., 2007; Hernández-Montoya et al., 2012); non-quinone EAC_{POM} and EDC_{POM} would likely be larger with smaller pH values (Aeschbacher et al., 2012; Fimmen et al., 2007; Hernández-Montoya et al., 2012). Moreover, it is likely that any relation between the N:C and S:C ratio and non-quinone EAC_{POM} and EDC_{POM} is confounded by the dependence of these element ratios and the quinone EAC_{POM} and EDC_{POM} on the degree of decomposition (Biester et al., 2014; see below).

4.2. Vegetation Chemistry and Decomposition Cause the Decoupling of Peat EAC_{POM} and EDC_{POM}

The decoupling of peat EAC_{POM} and EDC_{POM} (Figure 2b) can be explained by the joint effects of vegetation polymeric phenol contents and transformation of phenols to quinones during decomposition (Aeschbacher et al., 2012). It has been suggested that undecomposed plant-derived polymeric aromatics, such as lignin, have large contents of phenols, but small contents of quinones, which results in an initially large EDC, but small EAC (Aeschbacher et al., 2012). Decomposition and oxidation of the polymeric phenols decrease their fraction, but can increase the relative (and absolute) amount of quinones (Aeschbacher et al., 2012; Bolton et al., 2018; LaCroix et al., 2020). These mechanisms have four important implications: First, undecomposed samples have a maximum EDC, second, this maximum EDC varies depending on the vegetation polymeric phenol content, third, decomposition of polymeric phenols decreases the EDC and increases the EAC (Aeschbacher et al., 2012), and fourth, the initial EDC defines the maximum potential EAC of a sample. This explains why a decoupling of the EAC and EDC can be observed for humic and fulvic acids and DOM (Aeschbacher et al., 2012). Our measurements fit into the EDC-EAC gradient observed for humic and fulvic acids and DOM (Figure S20 in Supporting Information S1) and we therefore conclude that the decoupling of peat EAC_{POM} and EDC_{POM} is caused by the same mechanisms.

4.3. The Degree of Decomposition Confounds How the H:C Ratio Represents Phenols and Quinones

In contrast to Aeschbacher et al. (2012), we found only a weak relation between the EAC_{POM} and the H:C ratio. In Aeschbacher et al. (2012), a large H:C ratio indicates a smaller polymeric phenol and quinone content, but also a larger polysaccharide content because the H:C ratio is related to the O:C ratio (Figure 3). In contrast, for our peat POM samples, a large H:C ratio is not indicative for a larger polysaccharide content because it could also represent strongly decomposed samples with high lipid content (Figure 3a). This confounds how the H:C ratio represents polymeric phenols and quinones because peat samples with the same large H:C ratio tend to have a smaller EAC_{POM} if they contain a larger amount of lipids and smaller amount of polysaccharides (smaller O:C

ratio). This indicates that strongly decomposed, lipid rich, peat has fewer polymeric phenols and quinones than undecomposed peat. In other words, for the peat POM samples, the same H:C ratio can represent samples with either large O:C ratio or small O:C ratio, corresponding either to relatively undecomposed samples rich in polysaccharides and phenols and quinones or to strongly decomposed samples rich in lipids, but depleted in phenols and quinones (Bader et al., 2018; Kim et al., 2003; Leifeld et al., 2012). This interpretation is also supported by the joint relation of the H:C and O:C ratio to the EAC_{POM} in our regression models and by negative coefficients for MIRS variables representing lipids (Table 3, Figure S12 in Supporting Information S1). Thus, since differences in the O:C ratio are linked to differences in the EAC_{POM}, and since such samples are present within our data set, we found a weaker relation of the EAC_{POM} to the H:C ratio. It is likely that the same pattern caused the relative weak relation Tan et al. (2017) observed for the EAC of humic and fulvic acids to the H:C ratio.

4.4. Decomposition Indicators Are Poorly Related to Phenols and Quinones

We argue that many peat decomposition indicators are only weakly related to the EAC_{POM} and EDC_{POM} because they are not optimal descriptors of the polymeric phenol and quinone content. The O:C ratio is an indicator of the polysaccharide content and strongly related to all other decomposition indicators we analyzed (Pearson correlations of the O:C ratio with the N:C ratio, $HI_{1630/1090}$, and C_{OX} are −0.68, −0.82, and 0.87, respectively). If we focus on how these indicators describe the degree of decomposition, there is the same confounding as described above, but viewed from a different perspective: for strongly decomposed peat (small O:C ratio), the indicators cannot distinguish between peat with large content of polymeric quinones and phenols on the one hand (small H:C ratio) and strongly decomposed peat rich in lipids, but depleted in phenols and quinones (large H:C ratio) on the other hand. For this reason, the EAC_{POM} can vary considerably across a broad range of $HI_{1630/1090}$ and N:C ratios, as observed in our peat samples (Figure S11 in Supporting Information S1).

For the EDC_{POM}, this confounding effect is less relevant since the EDC_{POM} is negatively affected by decomposition, irrespective if the resulting peat is rich in lipids or polymeric quinones, as mentioned above (Bolton et al., 2018; Fenner & Freeman, 2011). This is evident from the stronger relation of the EDC_{POM} to the N:C ratio ($\rho = -0.69$). Nevertheless, since samples with a small O:C ratio that are rich in polymeric quinones and phenols have a larger EDC_{POM}, and since the $HI_{1630/1090}$ and C_{OX} do separate these samples less clearly from the lipid rich samples than the N:C ratio (Figure S11 in Supporting Information S1), the relation of both the $HI_{1630/1090}$ and C_{OX} is also weak for the EDC_{POM}.

4.5. Which Factors Determine the Polymeric Phenol and Quinone Content of Decomposed POM?

Which factors determine if a sample with a larger degree of decomposition is either rich in polymeric quinones and phenols—thus having a larger EAC_{POM} and EDC_{POM}—or rich in lipids—thus having the minimal EAC_{POM} and EDC_{POM}? Both, differences in vegetation chemistry and decomposition, may result in the observed differences in lipid versus polymeric quinone and phenol content.

Even though we cannot definitely disentangle both factors based on our data—we neither have complete information about the peat forming vegetation, nor the actual predominant decomposition processes—there is some evidence how both contribute. First of all, the samples with the smallest H:C ratio probably contain larger amounts of wood and root remains from trees and shrubs (e.g., both Lutose sites, especially the deepest samples (Heffernan et al., 2020); P. Brunswick (Broder et al., 2012); Mer Bleue, deepest sample (Elliott et al., 2012)) which is a plausible explanation for their large EAC_{POM}. In contrast, samples with approximately the same O:C ratio, but a larger H:C ratio are probably formed by sedges and (minerotrophic) *Sphagnum* mosses (samples from both fen sites [Touxi, Dongtu], or from the Patagonian bog [SKY I-1 and SKY I-6]) and likely strongly decomposed (Touxi, Dongtu) or known to be strongly decomposed (Both SKY I sites and SKY II, Broder et al. (2012); Mathijssen et al. (2019)). Second, intense aerobic decomposition of peat under drainage results in a larger H:C ratio, whereas less oxic conditions result in a decrease of the H:C ratio during decomposition (Leifeld et al., 2012). A plausible and likely explanation therefore is that aerobic decomposition of POM initially rich in polymeric phenols results in a large amount of quinones and therefore a large EAC_{POM}, whereas *intense* aerobic decomposition of POM that already had small initial amounts of polymeric phenols results in a large relative amount of lipids. Conversely, anaerobic decomposition may conserve initial polymeric phenols and quinones and thus EAC_{POM}

and EDC_{POM} (see below). This means that both vegetation chemistry and intensity of aerobic decomposition contribute to the observed pattern.

4.6. Differential Effects of Decomposition on Peat EAC_{POM}

The hypothesis that vegetation chemistry and decomposition intensity together change peat phenols and quinone content can help resolving the apparent contradiction we have produced: Partial oxidation of phenols to quinones during decomposition increases the EAC_{POM} (Aeschbacher et al., 2012; Tan et al., 2017; Walpen, Getzinger, et al., 2018), but typical MIRS-derived decomposition indicators such as the amount of lipids, unbonded OH groups, and aromatic backbone structures (Artz et al., 2008; Cocozza et al., 2003) are negatively related to the EAC_{POM} (Table 3). According to our conceptual understanding, the contradiction is only apparent: Aerobic decomposition of POM initially rich in polymeric phenols and quinones increases the amount of quinones (Aeschbacher et al., 2012), as indicated by larger amounts of carbonyl groups (Table 3). Intense aerobic decomposition of POM with initially low amounts of polymeric phenols and quinones (and hence larger amounts of polysaccharides) results in the mineralization of polysaccharides, phenols and quinones and the accumulation of lipids (Fenner & Freeman, 2011; Leifeld et al., 2012). Thus, if a specific peat contains large amounts of lipids and has an amorphous structure, this indicates that it also contains low amounts of polymeric phenols and quinones because it experienced intense decomposition.

4.7. A Conceptual Model for Peat EAC_{POM} and EDC_{POM}

To summarize our findings, we propose the conceptual model shown in Figure 4. We hypothesize that both the polymeric phenol content of the peat forming vegetation and the intensity of decomposition processes are the most important factors controlling the EDC_{POM} and EAC_{POM} of peat. Moreover, both factors likely interact since peat with initially large amounts of polymeric phenols has a smaller decomposition rate (Bengtsson et al., 2018).

Wood and roots from trees and shrubs are probably the plant remains with the largest fraction of polymeric phenols (Benner et al., 1984; Hodgkins et al., 2018; Straková et al., 2010; H. Wang et al., 2015; Williams et al., 1998), whereas other vascular plants and mosses have variable and partly smaller amounts of polymeric phenols (Bengtsson et al., 2018; Scheffer et al., 2001; Straková et al., 2010; H. Wang et al., 2015; Williams et al., 1998; Zak et al., 2019). For this reason, peat with larger contributions of wood or roots, for example, from shrubs (and potentially some graminoid or moss species), likely has the largest initial EDC_{POM} and upon decomposition the largest potential EAC_{POM} (Figure 4 and Figure S21 in Supporting Information S1). We propose that standardized measurements of electrochemical properties for different peat forming species are required to provide a quantitative basis for this hypothesis.

Under anoxic conditions, low phenol oxidase activities and the effects this has on other enzymes required for biomass breakdown (Fenner & Freeman, 2011) make peat material keep its initial EDC_{POM} and EAC_{POM}. In addition, quinone formation by partial oxidation is limited under such conditions, such that the EDC_{POM} should be relative large, whereas the EAC_{POM} remains smaller (Figure 4 and Figure S21 in Supporting Information S1). A factor that may decrease both the EAC_{POM} and EDC_{POM} under such conditions are condensation reactions (Bolton et al., 2018; Heitmann & Blodau, 2006; Hotta et al., 2002; Olk et al., 2006; Uchimiya & Stone, 2009; Yu et al., 2016; Zhao et al., 2020). Conversely, faster degradation of polysaccharides may increase the EAC_{POM} and EDC_{POM} since this results in a relative increase of phenols and quinones (Benner et al., 1984). However, it remains currently unclear to which extent both factors may play a role under anoxic conditions. Thus, we assume that under anoxic conditions the initial vegetation properties largely control peat electrochemical properties.

Under oxic conditions, increased phenol oxidase activities result in an oxidative transformation of polymeric phenols to quinones (Bolton et al., 2018; Fenner & Freeman, 2011; Schellekens et al., 2015). This can increase the EAC_{POM} and decrease the EDC_{POM}. If under such oxic conditions the mineralization of polymeric phenols, coupling reactions (Bolton et al., 2018; Hotta et al., 2002; Johnson et al., 2015; Zhao et al., 2020) and other condensation reactions (Bolton et al., 2018; Heitmann & Blodau, 2006; Olk et al., 2006; Yu et al., 2016) are further facilitated, for example, by warmer temperatures, large concentrations of nutrients, large amounts of labile OM, high pH values, (Bragazza & Freeman, 2007; Bowring et al., 2020; Fenner & Freeman, 2011; Kang et al., 2018), both the EAC_{POM} and EDC_{POM} may decrease (Figure 4 and Figure S21 in Supporting Information S1). Intense break-down of cell wall structures (as implied by our regression models for the EDC_{POM} and EAC_{POM}) may has

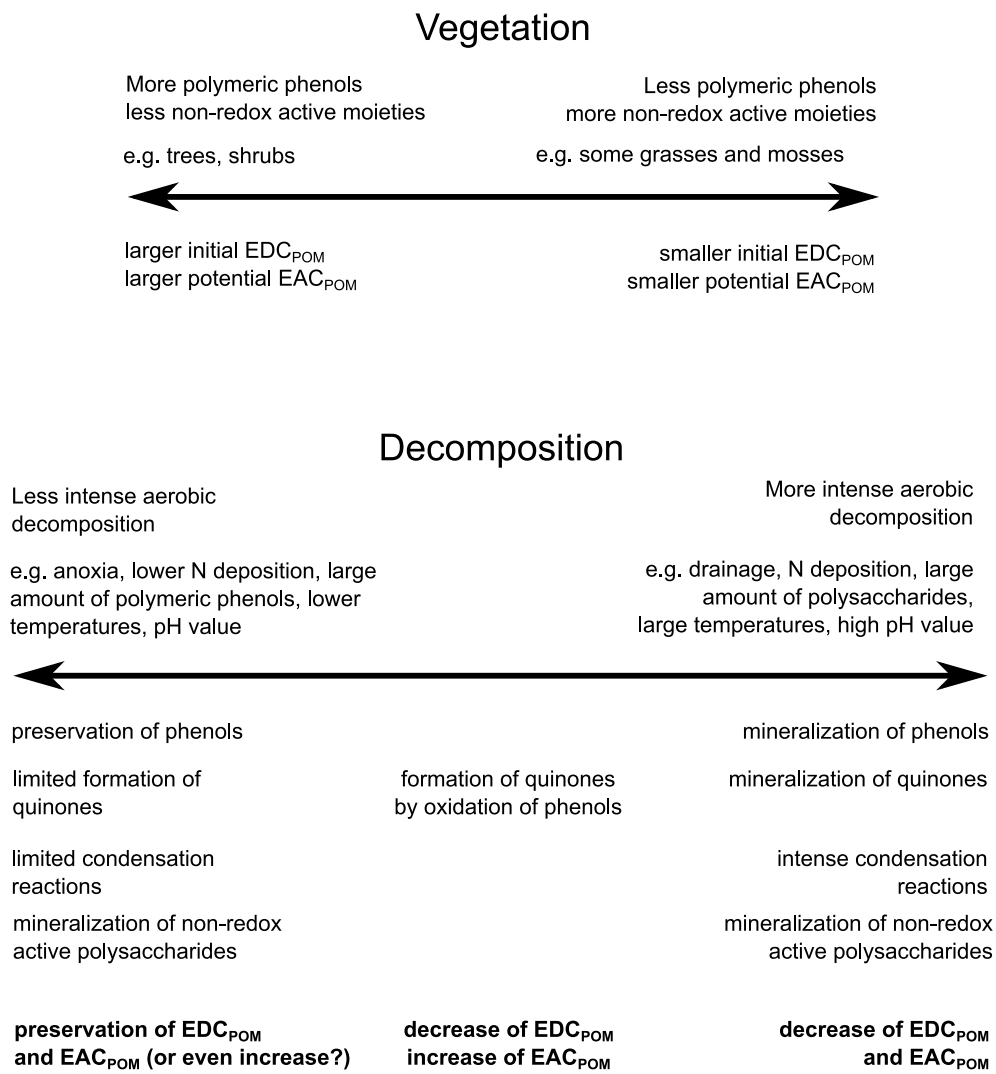

Figure 4. Conceptual description of the assumed effects of vegetation chemistry (polymeric phenol content) and decomposition pathways and intensity on peat chemistry and its EAC and EDC. Note that the assignment of plant taxa and their polymeric phenol contents is only an example as the chemical properties may be highly diverse within taxa (Bengtsson et al., 2018).

an important role since it increases the surface of the polymeric phenols exposed for oxidation or condensation reactions (Tsuneda et al., 2001). In addition, different vegetation has different types of polymeric phenols and it is assumed that *Sphagnum* phenols decompose faster than phenols of shrubs (H. Wang et al., 2015). For this reason, the EDC_{POM} and EAC_{POM} of *Sphagnum* peat may decrease at a larger rate during oxic decomposition than for peat with more contribution by shrubs or trees (H. Wang et al., 2015). Just as under anoxic conditions, a decrease in the EAC_{POM} and EDC_{POM} may be offset by faster mineralization of polysaccharides than polymeric phenols (Benner et al., 1984). However, again it remains currently unclear to which extent this factor and also condensation reactions play a role.

Thus, we assume that oxic conditions increase the EAC_{POM} at the expense of the EDC_{POM}. The initial content of polymeric phenols defines the maximum EAC_{POM} peat can attain throughout this process which results in variable responses of the peat EAC_{POM} and EDC_{POM} to decomposition. Intense aerobic decomposition, especially of material with low initial amounts of polymeric phenols, may even decrease the EAC due to mineralization and condensation of polymeric phenols.

4.8. MIRS-Based Regression Models Can Predict Peat EAC_{POM}

We suggest that our modeling approach is a proof-of-concept that peat EAC_{POM} can be predicted from MIRS. The MIRS-based model had the smallest average RMSE, albeit the RMSE for both the MIRS-based model and the element ratio-based model were relatively large and their 95%-posterior intervals broad and strongly overlapping. During graphical model validation, we observed that the element ratio-based model had a considerably larger bias than the MIRS-based model (Figure S15 in Supporting Information S1), suggesting that the MIRS-based model overall is more robust.

In contrast to this, both element ratio-based and MIRS-based regression models failed to adequately capture the variability in the EDC_{POM}. Since the EDC_{POM} of our samples in their oxidized state was smaller, the relative large predictive uncertainties turn both models unsuitable for practical applications.

5. Conclusions

Our research question was how peat chemistry relates to its EAC_{POM} and EDC_{POM} and how decomposition changes both. Based on our results, we hypothesize a conceptual model that describes how vegetation chemistry and intensity of aerobic decomposition control peat EAC_{POM} and EDC_{POM}. Undecomposed peat formed by vegetation rich in polymeric phenols has the largest EDC_{POM}. Decomposition of such material results in peat with the largest EAC_{POM}, but decreases the EDC_{POM}. In contrast, peat formed by vegetation with small amounts of polymeric phenols generally has a smaller EAC_{POM} and EDC_{POM}. Especially for such material, intense decomposition not only decreases the EDC_{POM}, but potentially also the EAC_{POM}. This model can plausibly explain the large variability in the relation of the EAC_{POM} and EDC_{POM} to peat chemical properties, decomposition indicators, and molecular structures, as well as the high intra-site variability and decoupling of the EAC_{POM} and EDC_{POM}. Finally, we provide a proof-of-concept that MIRS-based regression models may be at least suitable as screening tools to predict peat EAC_{POM}.

Our study has four inherent limitations: First, it is difficult to completely exclude contributions of iron to our estimates for the EAC_{POM} and EDC_{POM}. Second, we derived our conceptual understanding on purely observational data without experimental control. Third, we had only limited data on palaeovegetation and thus could only partly establish direct links between vegetation and peat chemistry. Fourth, to link our conceptual model to in situ processes occurring in peatlands (e.g., suppression of methanogenesis), it will be important to understand how in situ conditions modulate the EAC_{POM} and EDC_{POM} and its availability to microbes.

Nevertheless, our results imply that peat EAC_{POM} and EDC_{POM} can be spatially and temporally highly variable and that it is difficult to predict based on peat bulk properties. This furthermore implies that the potential for CH_4 suppression due to POM reduction may be similarly variable and difficult to predict.

Therefore, spatially resolved measurements or the incorporation of our hypothesized conceptual understanding into process models are required for the accurate quantification of peat EAC_{POM} and EDC_{POM} and their potential effects on redox processes, particularly CH_4 formation.

Data Availability Statement

Data and code to reproduce this document are available as research compendium on Zenodo (Teickner et al., 2021) and GitHub (https://github.com/henningte/redoxpeat). In addition, the MIRS-based reference models based on Bayesian regularization for both the EAC_{POM} and EDC_{POM} are available via the R package irpeat (Teickner & Hodgkins, 2021). These models can be used for predictions with own MIRS data.

Acknowledgments
For their support during sample collection/provision, we would like to thank Svenja Agethen (DE), Werner Borken (SKY I-1, SKY I-6), Tanja Broder (PBR, SKY II, LT, MK), Mariusz Gałka (LT, MK), Liam Heffernan (LP, LB), Norbert Hölzel (KR, ISH), Annkathrin Hömberg (TX, DT), Tim Moore (MB), Sindy Wagner (BB), Tim-Martin Wertebach (KR, ISH), and Zhi-Guo Yu (TX, DT). Analyses of this study were carried out in the laboratory of the Institute of Landscape Ecology. Svenja Agethen and Michael Sander provided analytical support. The assistance of Ulrike Berning-Mader, Madeleine Supper, Victoria Ratachin, and numerous student assistants is greatly acknowledged. We thank Dr. Hendrik Wetzel, Fraunhofer Institute for Applied Polymer Research, Dept. Starch Modification/Molecular Properties, Potsdam, Germany, for analysis of O and H. The workflow was reproduced by the Reproducible Research Support Service of the University of Münster. We thank two anonymous reviewers whose comments helped to improve the manuscript. This Study was funded by the Deutsche Forschungsgemeinschaft (DFG, German Research Foundation) grant no. KN 929/12–1 to Klaus-Holger Knorr; Chuanyu Gao was supported by the Youth Innovation Promotion Association CAS (No. 2020235). Open access funding enabled and organized by Projekt DEAL.

References

Aeschbacher, M., Graf, C., Schwarzenbach, R. P., & Sander, M. (2012). Antioxidant properties of humic substances. *Environmental Science & Technology*, *46*(9), 4916–4925. https://doi.org/10.1021/es300039h

Aeschbacher, M., Sander, M., & Schwarzenbach, R. P. (2010). Novel electrochemical approach to assess the redox properties of humic substances. *Environmental Science & Technology*, *44*(1), 87–93. https://doi.org/10.1021/es902627p

Aeschbacher, M., Vergari, D., Schwarzenbach, R. P., & Sander, M. (2011). Electrochemical analysis of proton and electron transfer equilibria of the reducible moieties in humic acids. *Environmental Science & Technology*, *45*(19), 8385–8394. https://doi.org/10.1021/es201981g

Artz, R. R., Chapman, S. J., Jean Robertson, A. H., Potts, J. M., Laggoun-Défarge, F., Gogo, S., et al. (2008). FTIR spectroscopy can be used as a screening tool for organic matter quality in regenerating cutover peatlands. *Soil Biology and Biochemistry*, *40*(2), 515–527. https://doi.org/10.1016/j.soilbio.2007.09.019

Bader, C., Müller, M., Schulin, R., & Leifeld, J. (2018). Peat decomposability in managed organic soils in relation to land use, organic matter composition and temperature. *Biogeosciences*, *15*(3), 703–719. https://doi.org/10.5194/bg-15-703-2018

Bai, Y., Sun, T., Angenent, L. T., Haderlein, S. B., & Kappler, A. (2020). Electron hopping enables rapid electron transfer between quinone-/hydroquinone-containing organic molecules in microbial iron(III) mineral reduction. *Environmental Science & Technology*, *54*(17), 10646–10653. https://doi.org/10.1021/acs.est.0c02521

Bellocchi, G., Rivington, M., Donatelli, M., & Matthews, K. (2010). Validation of biophysical models: Issues and methodologies. A review. *Agronomy for Sustainable Development*, *30*(1), 109–130. https://doi.org/10.1051/agro/2009001

Bengtsson, F., Rydin, H., & Hájek, T. (2018). Biochemical determinants of litter quality in 15 species of Sphagnum. *Plant and Soil*, *425*(1–2), 161–176. https://doi.org/10.1007/s11104-018-3579-8

Benner, R., Maccubbin, A. E., & Hodson, R. E. (1984). Anaerobic biodegradation of the lignin and polysaccharide components of lignocellulose and synthetic lignin by sediment microflora. *Applied and Environmental Microbiology*, *47*(5), 998–1004. https://doi.org/10.1128/aem.47.5.998-1004.1984

Biester, H., Knorr, K.-H., Schellekens, J., Basler, A., & Hermanns, Y.-M. (2014). Comparison of different methods to determine the degree of peat decomposition in peat bogs. *Biogeosciences*, *11*(10), 2691–2707. https://doi.org/10.5194/bg-11-2691-2014

Blodau, C. (2011). Thermodynamic control on terminal electron transfer and methanogenesis. In P. G. Tratnyek, T. J. Grundl, & S. B. Haderlein (Eds.), *Aquatic redox chemistry* (Vol. 1071, pp. 65–83). American Chemical Society. https://doi.org/10.1021/bk-2011-1071.ch004

Blodau, C., Mayer, B., Peiffer, S., & Moore, T. R. (2007). Support for an anaerobic sulfur cycle in two Canadian peatland soils. *Journal of Geophysical Research*, *112*(G2), 19. https://doi.org/10.1029/2006JG000364

Bolton, J. L., Dunlap, T. L., & Dietz, B. M. (2018). Formation and biological targets of botanical o-quinones. *Food and Chemical Toxicology: An international Journal Published for the British Industrial Biological Research Association*, *120*, 700–707. https://doi.org/10.1016/j.fct.2018.07.050

Bowring, S. P. K., Lauerwald, R., Guenet, B., Zhu, D., Guimberteau, M., Regnier, P., et al. (2020). ORCHIDEE MICT-LEAK (r5459), a global model for the production, transport, and transformation of dissolved organic carbon from Arctic permafrost regions–Part 2: Model evaluation over the Lena River basin. *Geoscientific Model Development*, *13*(2), 507–520. https://doi.org/10.5194/gmd-13-507-2020

Bragazza, L., & Freeman, C. (2007). High nitrogen availability reduces polyphenol content in Sphagnum peat. *The Science of the Total Environment*, *377*(2–3), 439–443. https://doi.org/10.1016/j.scitotenv.2007.02.016

Broder, T., Blodau, C., Biester, H., & Knorr, K. H. (2012). Peat decomposition records in three pristine Ombrotrophic bogs in southern Patagonia. *Biogeosciences*, *9*(4), 1479–1491. https://doi.org/10.5194/bg-9-1479-2012

Cocozza, C., D'Orazio, V., Miano, T. M., & Shotyk, W. (2003). Characterization of solid and aqueous phases of a peat bog profile using molecular fluorescence spectroscopy, ESR and FT-IR, and comparison with physical properties. *Organic Geochemistry*, *34*(1), 49–60. https://doi.org/10.1016/S0146-6380(02)00208-5

Danielson, J. J., & Gesch, D. B. (2010). *Global multi-resolution terrain elevation data 2010 (GMTED2010)*. https://doi.org/10.3133/ofr20111073

Drollinger, S., Knorr, K.-H., Knierzinger, W., & Glatzel, S. (2020). Peat decomposition proxies of Alpine bogs along a degradation gradient. *Geoderma*, *369*, 114331. https://doi.org/10.1016/j.geoderma.2020.114331

El Mansouri, N.-E., & Salvadó, J. (2007). Analytical methods for determining functional groups in various technical lignins. *Industrial Crops and Products*, *26*(2), 116–124. https://doi.org/10.1016/j.indcrop.2007.02.006

Elliott, S. M., Roe, H. M., & Patterson, R. T. (2012). Testate amoebae as indicators of hydroseral change: An 8500 year record from Mer Bleue Bog, eastern Ontario, Canada. *Quaternary International*, *268*, 128–144. https://doi.org/10.1016/j.quaint.2011.08.020

Engel, J., Gerretzen, J., Szymańska, E., Jansen, J. J., Downey, G., Blanchet, L., & Buydens, L. M. (2013). Breaking with trends in pre-processing? *TrAC Trends in Analytical Chemistry*, *50*, 96–106. https://doi.org/10.1016/j.trac.2013.04.015

Fenner, N., & Freeman, C. (2011). Drought-induced carbon loss in peatlands. *Nature Geoscience*, *4*(12), 895–900. https://doi.org/10.1038/ngeo1323

Ferragina, A., de los Campos, G., Vazquez, A. I., Cecchinato, A., & Bittante, G. (2015). Bayesian regression models outperform partial least squares methods for predicting milk components and technological properties using infrared spectral data. *Journal of Dairy Science*, *98*(11), 8133–8151. https://doi.org/10.3168/jds.2014-9143

Fick, S. E., & Hijmans, R. J. (2017). WorldClim 2: New 1–km spatial resolution climate surfaces for global land areas. *International Journal of Climatology*, *37*(12), 4302–4315. https://doi.org/10.1002/joc.5086

Fimmen, R. L., Cory, R. M., Chin, Y.-P., Trouts, T. D., & McKnight, D. M. (2007). Probing the oxidation–reduction properties of terrestrially and microbially derived dissolved organic matter. *Geochimica et Cosmochimica Acta*, *71*(12), 3003–3015. https://doi.org/10.1016/j.gca.2007.04.009

Frolking, S., Talbot, J., Jones, M. C., Treat, C. C., Kauffman, J. B., Tuittila, E.-S., & Roulet, N. (2011). Peatlands in the Earth's 21st century climate system. *Environmental Reviews*, *19*(NA), 371–396. https://doi.org/10.1139/a11-014

Gao, C., Sander, M., Agethen, S., & Knorr, K.-H. (2019). Electron accepting capacity of dissolved and particulate organic matter control CO_2 and CH_4 formation in peat soils. *Geochimica et Cosmochimica Acta*, *245*, 266–277. https://doi.org/10.1016/j.gca.2018.11.004

Heffernan, L., Estop-Aragonés, C., Knorr, K.-H., Talbot, J., & Olefeldt, D. (2020). Long–term impacts of permafrost thaw on carbon storage in peatlands: Deep losses offset by surficial accumulation. *Journal of Geophysical Research: Biogeosciences*, *125*(3), 457. https://doi.org/10.1029/2019JG005501

Heitmann, T., & Blodau, C. (2006). Oxidation and incorporation of hydrogen sulfide by dissolved organic matter. *Chemical Geology*, *235*(1–2), 12–20. https://doi.org/10.1016/j.chemgeo.2006.05.011

Hernández-Montoya, V., Alvarez, L. H., Montes-Morán, M. A., & Cervantes, F. J. (2012). Reduction of quinone and non-quinone redox functional groups in different humic acid samples by Geobacter sulfurreducens. *Geoderma*, *183–184*, 25–31. https://doi.org/10.1016/j.geoderma.2012.03.007

Hodgkins, S. B., Richardson, C. J., Dommain, R., Wang, H., Glaser, P. H., Verbeke, B., et al. (2018). Tropical peatland carbon storage linked to global latitudinal trends in peat recalcitrance. *Nature Communications*, *9*(1), 3640. https://doi.org/10.1038/s41467-018-06050-2

Hotta, H., Nagano, S., Ueda, M., Tsujino, Y., Koyama, J., & Osakai, T. (2002). Higher radical scavenging activities of polyphenolic antioxidants can be ascribed to chemical reactions following their oxidation. *Biochimica et Biophysica Acta (BBA)-General Subjects*, *1572*(1), 123–132. https://doi.org/10.1016/S0304-4165(02)00285-4

Huffman Laboratories & Soil Biochemistry Laboratory University of Minnesota. (NA). *Elemental compositions and stable isotopic ratios of IHSS samples*. Retrieved from http://humic-substances.org/elemental-compositions-and-stable-isotopic-ratios-of-ihss-samples/

Johnson, K., Purvis, G., Lopez-Capel, E., Peacock, C., Gray, N., Wagner, T., et al. (2015). Towards a mechanistic understanding of carbon stabilization in manganese oxides. *Nature Communications*, *6*, 7628. https://doi.org/10.1038/ncomms8628

Kang, H., Kwon, M. J., Kim, S., Lee, S., Jones, T. G., Johncock, A. C., et al. (2018). Biologically driven DOC release from peatlands during recovery from acidification. *Nature Communications*, *9*(1), 3807. https://doi.org/10.1038/s41467-018-06259-1

Keller, J. K., & Takagi, K. K. (2013). Solid-phase organic matter reduction regulates anaerobic decomposition in bog soil. *Ecosphere*, *4*(5), 1–12. https://doi.org/10.1890/ES12-00382.1

Kim, S., Kramer, R. W., & Hatcher, P. G. (2003). Graphical method for analysis of ultrahigh-resolution broadband mass spectra of natural organic matter, the van Krevelen diagram. *Analytical Chemistry*, *75*(20), 5336–5344. https://doi.org/10.1021/ac034415p

Klüpfel, L., Piepenbrock, A., Kappler, A., & Sander, M. (2014). Humic substances as fully regenerable electron acceptors in recurrently anoxic environments. *Nature Geoscience*, *7*(3), 195–200. https://doi.org/10.1038/ngeo2084

Kubo, S., & Kadla, J. F. (2005). Hydrogen bonding in lignin: A Fourier transform infrared model compound study. *Biomacromolecules*, *6*(5), 2815–2821. https://doi.org/10.1021/bm050288q

LaCroix, R. E., Walpen, N., Sander, M., Tfaily, M. M., Blanchard, J. L., & Keiluweit, M. (2020). Long-Term warming decreases redox capacity of soil organic matter. *Environmental Science and Technology Letters*, *8*, 92–97. https://doi.org/10.1021/acs.estlett.0c00748

Larina, N. S., Larin, S. I., & Moiseenko, T. I. (2013). Geochemical differentiation in the stratigraphy of a peat bed as an indicator of its evolution in the Holocene. *Geochemistry International*, *51*(2), 129–139. https://doi.org/10.1134/S0016702913020067

Lau, M. P., Sander, M., Gelbrecht, J., & Hupfer, M. (2015). Solid phases as important electron acceptors in freshwater organic sediments. *Biogeochemistry*, *123*(1–2), 49–61. https://doi.org/10.1007/s10533-014-0052-5

Lau, M. P., Sander, M., Gelbrecht, J., & Hupfer, M. (2016). Spatiotemporal redox dynamics in a freshwater lake sediment under alternating oxygen availabilities: Combined analyses of dissolved and particulate electron acceptors. *Environmental Chemistry*, *13*(5), 826. https://doi.org/10.1071/EN15217

Leifeld, J., Klein, K., & Wüst-Galley, C. (2020). Soil organic matter stoichiometry as indicator for peatland degradation. *Scientific reports*, *10*(1), 7634. https://doi.org/10.1038/s41598-020-64275-y

Leifeld, J., Steffens, M., & Galego-Sala, A. (2012). Sensitivity of peatland carbon loss to organic matter quality. *Geophysical Research Letters*, *39*(14), L14704. https://doi.org/10.1029/2012gl051856

Limpens, J., Berendse, F., Blodau, C., Canadell, J. G., Freeman, C., Holden, J., et al. (2008). Peatlands and the carbon cycle: From local processes to global implications–A synthesis. *Biogeosciences*, *5*(5), 1475–1491. https://doi.org/10.5194/bg-5-1475-2008

Lipczynska-Kochany, E. (2018). Humic substances, their microbial interactions and effects on biological transformations of organic pollutants in water and soil: A review. *Chemosphere*, *202*, 420–437. https://doi.org/10.1016/j.chemosphere.2018.03.104

Loisel, J., Yu, Z., Beilman, D. W., Camill, P., Alm, J., Amesbury, M. J., et al. (2014). A database and synthesis of northern peatland soil properties and Holocene carbon and nitrogen accumulation. *The Holocene*, *24*(9), 1028–1042. https://doi.org/10.1177/0959683614538073

Lu, Q., Yuan, Y., Tao, Y., & Tang, J. (2015). Environmental pH and ionic strength influence the electron-transfer capacity of dissolved organic matter. *Journal of Soils and Sediments*, *15*(11), 2257–2264. https://doi.org/10.1007/s11368-015-1154-y

Lv, J., Han, R., Huang, Z., Luo, L., Cao, D., & Zhang, S. (2018). Relationship between molecular components and reducing capacities of humic substances. *ACS Earth and Space Chemistry*, *2*(4), 330–339. https://doi.org/10.1021/acsearthspacechem.7b00155

Masiello, C. A., Gallagher, M. E., Randerson, J. T., Deco, R. M., & Chadwick, O. A. (2008). Evaluating two experimental approaches for measuring ecosystem carbon oxidation state and oxidative ratio. *Journal of Geophysical Research*, *113*(G3), 39. https://doi.org/10.1029/2007JG000534

Mathijssen, P. J. H., Gałka, M., Borken, W., & Knorr, K.-H. (2019). Plant communities control long term carbon accumulation and biogeochemical gradients in a Patagonian bog. *The Science of the Total Environment*, *684*, 670–681. https://doi.org/10.1016/j.scitotenv.2019.05.310

Moore, T. R., Large, D., Talbot, J., Wang, M., & Riley, J. L. (2018). The stoichiometry of carbon, hydrogen, and oxygen in peat. *Journal of Geophysical Research: Biogeosciences*, *123*(10), 3101–3110. https://doi.org/10.1029/2018JG004574

Olk, D. C., Cassman, K. G., Schmidt-Rohr, K., Anders, M. M., Mao, J.-D., & Deenik, J. L. (2006). Chemical stabilization of soil organic nitrogen by phenolic lignin residues in anaerobic agroecosystems. *Soil Biology and Biochemistry*, *38*(11), 3303–3312. https://doi.org/10.1016/j.soilbio.2006.04.009

Piironen, J., Paasiniemi, M., & Vehtari, A. (2020). Projective inference in high-dimensional problems: Prediction and feature selection. *Electronic Journal of Statistics*, *14*(1), 2155–2197. https://doi.org/10.1214/20-EJS1711

Poisot, T. (2011). The digitize package: Extracting numerical data from scatterplots. *The R Journal*, *3*(1), 25. https://doi.org/10.32614/RJ-2011-004

Ratasuk, N., & Nanny, M. A. (2007). Characterization and quantification of reversible redox sites in humic substances. *Environmental Science & Technology*, *41*(22), 7844–7850. https://doi.org/10.1021/es071389u

Roberts, D. R., Bahn, V., Ciuti, S., Boyce, M. S., Elith, J., Guillera-Arroita, G., et al. (2017). Cross-validation strategies for data with temporal, spatial, hierarchical, or phylogenetic structure. *Ecography*, *40*(8), 913–929. https://doi.org/10.1111/ecog.02881

Rydin, H., Jeglum, J. K., & Bennett, K. D. (2013). *The biology of peatlands* (2nd ed.). Oxford University Press.

Sagerfors, J., Lindroth, A., Grelle, A., Klemedtsson, L., Weslien, P., & Nilsson, M. (2008). Annual CO_2 exchange between a nutrient-poor, minerotrophic, boreal mire and the atmosphere. *Journal of Geophysical Research*, *113*(G1), G01001. https://doi.org/10.1029/2006jg000306

Scheffer, R. A., van Logtestijn, R. S. P., & Verhoeven, J. T. A. (2001). Decomposition of Carex and Sphagnum litter in two mesotrophic fens differing in dominant plant species. *Oikos*, *92*(1), 44–54. https://doi.org/10.1034/j.1600-0706.2001.920106.x

Schellekens, J., Bindler, R., Martínez-Cortizas, A., McClymont, E. L., Abbott, G. D., Biester, H., et al. (2015). Preferential degradation of polyphenols from Sphagnum–4-Isopropenylphenol as a proxy for past hydrological conditions in Sphagnum-dominated peat. *Geochimica et Cosmochimica Acta*, *150*, 74–89. https://doi.org/10.1016/j.gca.2014.12.003

Schmidt, M., Gierlinger, N., Schade, U., Rogge, T., & Grunze, M. (2006). Polarized infrared microspectroscopy of single spruce fibers: Hydrogen bonding in wood polymers. *Biopolymers*, *83*(5), 546–555. https://doi.org/10.1002/bip.20585

signal developers (2014). *signal: Signal processing*. Retrieved from http://r-forge.r-project.org/projects/signal/

South, A. (2017). *rnaturalearth: World map data from natural earth*. Retrieved from https://CRAN.R-project.org/package=rnaturalearth

Straková, P., Anttila, J., Spetz, P., Kitunen, V., Tapanila, T., & Laiho, R. (2010). Litter quality and its response to water level drawdown in boreal peatlands at plant species and community level. *Plant and Soil*, *335*(1–2), 501–520. https://doi.org/10.1007/s11104-010-0447-6

Stuart, B. H. (2004). *Infrared spectroscopy: Fundamentals and applications*. *Analytical techniques in the sciences*: Wiley-Interscience. Retrieved from https://doi.org/10.1002/0470011149

Tamura, H., Goto, K., Yotsuyanagi, T., & Nagayama, M. (1974). Spectrophotometric determination of iron(II) with 1,10-phenanthroline in the presence of large amounts of iron(III). *Talanta*, *21*(4), 314–318. https://doi.org/10.1016/0039-9140(74)80012-3

Tan, W., Xi, B., Wang, G., Jiang, J., He, X., Mao, X., et al. (2017). Increased electron-accepting and decreased electron-donating capacities of soil humic substances in response to increasing temperature. *Environmental Science & Technology*, *51*(6), 3176–3186. https://doi.org/10.1021/acs.est.6b04131

Teickner, H. (2021). ir: A simple package to handle and preprocess infrared spectra. *Zenodo*. Retrieved from Zenodo. Retrieved from https://zenodo.org/record/5747170

Teickner, H., Chuanyu, G., & Knorr, K.-H. (2021). *Reproducible research compendium with R code and data for: "Electrochemical properties of peat particulate organic matter on a global scale: Relation to peat chemistry and degree of decomposition"*. https://doi.org/10.5281/zenodo.5792970

Teickner, H., & Hodgkins, S. B. (2021). *irpeat: Simple functions to analyze mid infrared spectra of peat samples*. Zenodo. https://doi.org/10.5281/zenodo.5792919

Tfaily, M. M., Cooper, W. T., Kostka, J. E., Chanton, P. R., Schadt, C. W., Hanson, P. J., et al. (2014). Organic matter transformation in the peat column at Marcell Experimental Forest: Humification and vertical stratification. *Journal of Geophysical Research: Biogeosciences*, *119*(4), 661–675. https://doi.org/10.1002/2013JG002492

Tipping, E., Somerville, C. J., & Luster, J. (2016). The C:N:P:S stoichiometry of soil organic matter. *Biogeochemistry*, *130*(1), 117–131. https://doi.org/10.1007/s10533-016-0247-z

Tsuneda, A., Thormann, M. N., & Currah, R. S. (2001). Modes of cell-wall degradation of *Sphagnum fuscum* by *Acremonium* cf. *curvulum* and *Oidiodendron maius*. *Canadian Journal of Botany*, *79*(1), 93–100. https://doi.org/10.1139/b00-149

Uchimiya, M., & Stone, A. T. (2009). Reversible redox chemistry of quinones: Impact on biogeochemical cycles. *Chemosphere*, *77*(4), 451–458. https://doi.org/10.1016/j.chemosphere.2009.07.025

Walpen, N., Getzinger, G. J., Schroth, M. H., & Sander, M. (2018). Electron-donating phenolic and electron-accepting Quinone moieties in peat dissolved organic matter: Quantities and redox transformations in the context of peat biogeochemistry. *Environmental Science & Technology*, *52*(9), 5236–5245. https://doi.org/10.1021/acs.est.8b00594

Walpen, N., Lau, M. P., Fiskal, A., Getzinger, G. J., Meyer, S. A., Nelson, T. F., et al. (2018). Oxidation of reduced peat particulate organic matter by dissolved oxygen: Quantification of apparent rate constants in the field. *Environmental Science & Technology*, *52*(19), 11151–11160. https://doi.org/10.1021/acs.est.8b03419

Wang, H., Richardson, C. J., & Ho, M. (2015). Dual controls on carbon loss during drought in peatlands. *Nature Climate Change*, *5*(6), 584–587. https://doi.org/10.1038/nclimate2643

Wang, M., Moore, T. R., Talbot, J., & Riley, J. L. (2015). The stoichiometry of carbon and nutrients in peat formation. *Global Biogeochemical Cycles*, *29*(2), 113–121. https://doi.org/10.1002/2014GB005000

Wertebach, T.-M., Knorr, K.-H., Lordieck, M., Tretiakov, N., Blodau, C., Hölzel, N., & Kleinebecker, T. (2016). Relationships between vegetation succession, pore water chemistry and CH_4 and CO_2 production in a transitional mire of Western Siberia (Tumen Oblast). *Wetlands*, *36*(5), 863–874. https://doi.org/10.1007/s13157-016-0798-8

Williams, C. J., Yavitt, J. B., Wieder, R. K., & Cleavitt, N. L. (1998). Cupric oxide oxidation products of northern peat and peat-forming plants. *Canadian Journal of Botany*, *76*(1), 51–62. https://doi.org/10.1139/b97-150

Worrall, F., Clay, G. D., Moody, C. S., Burt, T. P., & Rose, R. (2016). The effective oxidation state of a peatland. *Journal of Geophysical Research: Biogeosciences*, *121*(1), 145–158. https://doi.org/10.1002/2015JG003182

Worrall, F., Moody, C. S., Clay, G. D., Burt, T. P., & Rose, R. (2017). The flux of organic matter through a peatland ecosystem: The role of cellulose, lignin, and their control of the ecosystem oxidation state. *Journal of Geophysical Research: Biogeosciences*, *122*(7), 1655–1671. https://doi.org/10.1002/2016JG003697

Yu, Z.-G., Göttlicher, J., Steininger, R., & Knorr, K.-H. (2016). Organic sulfur and organic matter redox processes contribute to electron flow in anoxic incubations of peat. *Environmental Chemistry*, *13*(5), 816. https://doi.org/10.1071/EN15091

Yuan, Y., Cai, X., Tan, B., Zhou, S., & Xing, B. (2018). Molecular insights into reversible redox sites in solid-phase humic substances as examined by electrochemical in situ FTIR and two-dimensional correlation spectroscopy. *Chemical Geology*, *494*(1), 136–143. https://doi.org/10.1016/j.chemgeo.2018.07.029

Zak, D., Roth, C., Unger, V., Goldhammer, T., Fenner, N., Freeman, C., & Jurasinski, G. (2019). Unraveling the importance of polyphenols for microbial carbon mineralization in rewetted riparian peatlands. *Frontiers in Environmental Science*, *7*, 1521. https://doi.org/10.3389/fenvs.2019.00147

Zhao, Y., Xiang, W., Zhang, X., Xie, S., Yan, S., Wu, C., & Liu, Y. (2020). Mechanistic study on laccase-mediated formation of Fe-OM associations in peatlands. *Geoderma*, *375*, 114502. https://doi.org/10.1016/j.geoderma.2020.114502

References From the Supporting Information

Bååth, R. (2018). *Diagrams of distributions in the style of Kruschke (2011)*. Retrieved from https://github.com/rasmusab/distribution_diagrams

Bache, S. M., & Wickham, H. (2014). *magrittr: A forward-pipe operator for R*. Retrieved from https://CRAN.R-project.org/package=magrittr

Beleites, C., & Sergo, V. (2020). *hyperSpec: a package to handle hyperspectral data sets in R*. Retrieved from https://github.com/cbeleites/hyperSpec

Bivand, R., & Rundel, C. (2020). *rgeos: Interface to geometry engine-open source ("GEOS")*. Retrieved from https://CRAN.R-project.org/package=rgeos

Carpenter, B., Gelman, A., Hoffman, M. D., Lee, D., Goodrich, B., Betancourt, M., & Riddell, A. (2017). Stan: A probabilistic programming language. *Journal of Statistical Software*, *76*(1). https://doi.org/10.18637/jss.v076.i01

Gabry, J., Goodrich, B., & Lysy, M. (2019). *rstantools: Tools for developing R packages interfacing with "Stan"*. Retrieved from https://CRAN.R-project.org/package=rstantools

Gabry, J., Simpson, D., Vehtari, A., Betancourt, M., & Gelman, A. (2019). Visualization in Bayesian workflow. *Journal of the Royal Statistical Society: Series A (Statistics in Society)*, *182*(2), 389–402. Retrieved from http://arxiv.org/pdf/1709.01449v5/doi.org/10.1111/rssa.12378

Gelman, A., Carlin, J. B., Stern, H. S., Dunson, D. B., Vehtari, A., & Rubin, D. B. (2014). *Bayesian data analysis* (3rd ed.). CRC Press Taylor and Francis Group.

Goodrich, B., Gabry, J., Ali, I., & Brilleman, S. (2020). *rstanarm: Bayesian applied regression modeling via Stan*. Retrieved from https://mc-stan.org/rstanarm

Henry, L., & Wickham, H. (2020). *purrr: Functional programming tools*. Retrieved from https://CRAN.R-project.org/package=purrr

Hijmans, R. J. (2020). *raster: Geographic data analysis and modeling*. Retrieved from https://CRAN.R-project.org/package=raster

Kruschke, J. K. (2015). *Doing Bayesian data analysis: A tutorial with R, JAGS, and Stan* (2nd ed.). AP Academic Press/Elsevier.

Mevik, B.-H., Wehrens, R., & Liland, K. H. (2019). *pls: Partial least squares and principal component regression*. Retrieved from https://CRAN.R-project.org/package=pls

Moore, T. R., Bubier, J. L., & Bledzki, L. (2007). Litter decomposition in temperate peatland ecosystems: The effect of substrate and site. *Ecosystems*, *10*(6), 949–963. https://doi.org/10.1007/s10021-007-9064-5

Pebesma, E. (2018). Simple features for R: Standardized support for spatial vector data. *The R Journal*, *10*(1), 439. https://doi.org/10.32614/RJ-2018-009

Pebesma, E., & Bivand, R. (2005). *Classes and methods for spatial data in R. R News* (Vol. 5). (pp. 9–13). Retrieved from https://CRAN.R-project.org/doc/Rnews/

Pebesma, E., Mailund, T., & Hiebert, J. (2016). Measurement units in R. *The R Journal*, *8*(2), 486. https://doi.org/10.32614/RJ-2016-061

Pedersen, T. L. (2019). *ggforce: Accelerating "ggplot2"*. Retrieved from https://CRAN.R-project.org/package=ggforce

Piironen, J., Paasiniemi, M., Vehtari, A., Gabry, J., Bürkner, P.-C., & Colombo, M. (2019). *projpred: Projection predictive feature selection*. Retrieved from https://cloud.r-project.org/web/packages/projpred/index.html

Piironen, J., & Vehtari, A. (n.d.). *On the hyperprior choice for the global shrinkage parameter in the horseshoe prior*.

Piironen, J., & Vehtari, A. (2017). Comparison of Bayesian predictive methods for model selection. *Statistics and Computing*, *27*(3), 711–735. https://doi.org/10.1007/s11222-016-9649-y

R Core Team. (2020). *R: A language and environment for statistical computing*. R Foundation for Statistical Computing. Retrieved from https://www.R-project.org/

Scheffer, R. A., & Aerts, R. (2000). Root decomposition and soil nutrient and carbon cycling in two temperate fen ecosystems. *Oikos*, *91*(3), 541–549. https://doi.org/10.1034/j.1600-0706.2000.910316.x

Slowikowski, K. (2020). *ggrepel: Automatically position non-overlapping text labels with*. Retrieved from https://CRAN.R-project.org/package=ggrepel

Stan Development Team. (2020). *RStan: The R interface to Stan*. Retrieved from http://mc-stan.org/

Teickner, H. (2021). *ir: A simple package to handle and preprocess infrared spectra*. Zenodo. Retrieved from https://zenodo.org/record/5747170

Teickner, H., & Knorr, K.-H. (2020). *elco: Handling data on chemical element contents and isotope signatures*. Retrieved from https://github.com/henningte/elco

Ucar, I., Pebesma, E., & Azcorra, A. (2019). Measurement errors in R. *The R Journal*, *10*(2), 549. https://doi.org/10.32614/RJ-2018-075

Wickham, H. (2016). *ggplot2: Elegant graphics for data analysis*. Springer. https://doi.org/10.1007/978-3-319-24277-4

Wickham, H., François, R., Henry, L., & Müller, K. (2020). *dplyr: A grammar of data manipulation*. Retrieved from https://CRAN.R-project.org/package=dplyr

Wickham, H., & Henry, L. (2020). *tidyr: Tidy messy data*. Retrieved from https://CRAN.R-project.org/package=tidyr

Wilke, C. O. (2019). *cowplot: Streamlined plot theme and plot annotations for "ggplot2"*. Retrieved from https://CRAN.R-project.org/package=cowplot